



Title	Theoretical Study on Formation, Stability and Reaction of Small Water Clusters
Author(s)	Kuncoro, Handoko Setyo
Citation	大阪大学, 2013, 博士論文
Version Type	VoR
URL	https://doi.org/10.18910/26843
rights	
Note	

The University of Osaka Institutional Knowledge Archive : OUKA

<https://ir.library.osaka-u.ac.jp/>

The University of Osaka

Theoretical Study on Formation, Stability and Reaction of Small Water Clusters

(水分子クラスターの形成機構と安定性及び反応性に関する理論的研究)

Handoko Setyo Kuncoro

ハンドコ セティオ クンチョロ

February 2013

Division of Precision Science & Technology and Applied Physics
Graduate School of Engineering
Osaka University
大阪大学大学院工学研究科
精密科学・応用物理学専攻

Theoretical Study on Formation, Stability and Reaction of Small Water Clusters

(水分子クラスターの形成機構と安定性及び反応性に関する理論的研究)

Handoko Setyo Kuncoro

ハンドコ セティオ クンチョロ

February 2013

Division of Precision Science & Technology and Applied Physics

Graduate School of Engineering

Osaka University

大阪大学大学院工学研究科

精密科学・応用物理学専攻

Abstract

Dehumidification (dehydration) and cationic contaminations of small water clusters inside the membranes could degrade the proton exchange membrane fuel cell (PEMFC) performance. Some related quantities for the small water clusters have been evaluated. The first study deals with the formations, binding energies and monomer dipole moments of small water cluster systems $(\text{H}_2\text{O})_n$ with $n=1-12$, investigated by density functional theory (DFT) using B3LYP/6-311++(2d,2p) (chapter I and II). A method based on reactivity indices from Fukui function has been introduced to generate the initial structures of water clusters. Constantly adding one water molecule to water monomer has transformed the water cluster formations from linear ($n=2$), cyclic planar ($n=3-6$) to 3-dimensional ($n=7-12$) shapes. Concerning the local binding energy fluctuation effects on the average binding energy trend, the average binding energies of small water cluster systems converged asymptotically to the intermolecular binding of bulk water. Due to the total electronic energies, zero point energies and activation energies analyses, we have predicted that the cyclic planar is the most stable formation for water hexamers to compete with the cage and the book formations. In the second research (chapter III), some ionic effects on small water cluster systems formed around sodium(I), calcium(II), and iron(II) cations have been studied using the DFT. By assuming that the number of water molecules in the first and the second water layers are 6 and 12, respectively, it is shown that (i) the Ca(II) aqueous cluster shrinks and its volume becomes similar to that of a pure $(\text{H}_2\text{O})_{18}$ cluster whereas the Fe(II) and Na(I) aqueous clusters expand; (ii) owing to the inter dipole water interactions induced by the ion in the second water layer binding, the ionization strength of the Ca(II) aqueous cluster is close to that of Fe(II) but sufficiently higher than that of Na(I); (iii) the isotropicity of s-type acceptor of Ca(II) and Na(I) MOs as the cause of the reduction in water rotational rigidity in the ion–water bonding has been clarified by analysing the donor-acceptor charge transfer and non-interacting kinetic energy. By considering the three ionic effects, we predict that the Ca(II) ion is one of the more competitive water cationic impurities in the PEMFC membrane. The third study (chapter IV) is about single water dissociation investigations which has revealed that the hollow shape of charge density of central Cr(III) makes the Cr-O bonds rigid as indicated by a higher activation energy for releasing one water molecule from $\text{Cr}[(\text{H}_2\text{O})_6]^{3+}$. The isotropic charge density of Fe(III) affects in lowering water rotational rigidities which is also responsible augmenting the activation. Here, the calculations had been performed based on first-principles study.

Contents

	pg
Chapter I Introduction	
1.1 Background	... 11
1.2 Problem	... 13
1.3 Objective	... 13
1.4 Methodology	... 14
1.5 Scope	... 14
1.6 Systematic	... 14
Chapter II The Formation of Small Water Cluster Systems	
2.1. Introduction to density functional theory (DFT)	... 16
2.2. Molecular active site	... 17
2.2.1. Electrostatic potential	... 17
2.2.2. Fukui indices	... 17
2.3. Atomic charge and monomer dipole moment	... 20
2.4. A case study on small water clusters formation	... 24
Chapter III The Stability of Small Water Cluster Systems	
3.1. Introduction to molecular structure optimization	... 33
3.2. Introduction to transition state optimization	... 35
3.3. A case study on molecular optimization and phase state of small water cluster systems	... 39
3.4. A case study on transition state of cage and cyclic water hexamers	... 41
Chapter IV Small Water Clusters Role in Fuel Cell Membrane	... 43
4.1. Computational method	... 44
4.2. Physical phase state and molecular binding strength	... 48
4.3. Volume expansion	... 51
4.4. Water dynamic and proton transport	... 54
4.5. An evaluation on cationic contaminants in the membrane	... 57

Chapter V	Single Water Dissociation Effect in Ion-exchange Reaction		
5.1.	Related applications	...	58
5.2.	Computational methods	...	59
5.3.	Hydration enthalpies	...	63
5.4.	Single dehydration mechanism and reaction products	...	67
Chapter VI	Conclusion		
6.1.	Summary	...	75
6.2.	Suggestion	...	79
	References	...	80
	Appendix: Gaussian 03 input program	...	89
CV	Curriculum vitae		
	List of publication	...	91
	List of international conference	...	92
	List of international collaboration workshop	...	93
	Provisional education and experiences	...	94
	Acknowledgments		

List of Figures

	pg
Chapter II	...
2.1. The monomer dipole moments of small water cluster with $n = 1$ to 8. The dashed lines in main figure are taken from experimental data for gas, liquid and solid phase. These studies have used APT charge in order to calculate the monomer dipole moment values.	... 24
2.2. The stability of eclipsed dimer is examined by scanning the energy profile as the H atoms are rotated (θ) from 0° to 180° with O atom as the center of rotation.	... 27
2.3. Water cluster formations are arranged from cluster structures with $n = 1-12$. The white color of water molecule is approaching molecule. The structures of hexamer ($n = 6$) and decamer ($n = 10$) are shown into 2 stable formations.	... 30
2.4. The average ($\overline{\Delta E_b}$) binding energies trend and local (ΔE_h) binding energy fluctuations for the most stable findings (linear dimer, cyclic planar trimer, cyclic planar tetramer, cyclic planar pentamer, cyclic planar hexamer, prism ₃₄ 3-D. heptamer, cubic-like 3-D. octamer, prism ₄₅ 3-D. nonamer, fish 3-D. decamer, asymmetric 3-D. undecamer, two-cubic-like 3-D. dodecamer) of small water cluster systems.	... 31
Chapter III	...
3.1. An illustration of potential energy surface in a simple reaction, including minimum energy of reactants, product (at equilibriums or stable structure), and an activation energies (at saddle point or transition structure).	... 37
3.2. (A1) Total energy relative in molecular optimization of $[\text{Ca}(\text{H}_2\text{O})_6]^{2+}$, (A2) optimized interatomic distances of $[\text{Ca}(\text{H}_2\text{O})_6]^{2+}$, (B1) total energy relative in molecular optimization of $[\text{Fe}(\text{H}_2\text{O})_6]^{2+}$, and (B2) optimized interatomic distances, of $[\text{Fe}(\text{H}_2\text{O})_6]^{2+}$ 38
3.3. Optimized structures of the $(\text{H}_2\text{O})_6$, $(\text{H}_2\text{O})_{12}$, and $(\text{H}_2\text{O})_{18}$ models. The cage like hexamer parts are shown by w1, w2, and	

w3 and the intermolecular H-bond distances are represented by H–O symbols.	...	39
3.4. The three stable formations of hexamer: cyclic, cage and book formations including their zero point energies, transition formations and the activation energies. The dashed line represents energy reference from cyclic hexamer.	...	41
Chapter IV		
4.1. Monomer dipole moments of small modeled water clusters [hexamer (H ₂ O) ₆ , dodecamer (H ₂ O) ₁₂ , and octadecamer (H ₂ O) ₁₈]. Experimental values [25] for the solid, liquid, and gas phases of bulk water are indicated by the corresponding horizontal lines.	...	49
4.2. The optimized structures of (a) Ca[(H ₂ O) ₆] ²⁺ (including the cation and water atomic charges) and (b) Ca[(H ₂ O) ₁₈] ²⁺ formed two water layers. The inner dashed line represents the first water layer and the outer dashed line represents the second water layer in the Ca[(H ₂ O) ₁₈] ²⁺ cluster.	...	49
4.3. Isosurface volumes of the total electronic density at contour 0.001 e.Bohr ⁻³ : (a) (H ₂ O) ₁₈ and (b) Ca[(H ₂ O) ₁₈] ²⁺ clusters.	...	52
4.4. (a) Main charge transfer of the Ca[(H ₂ O) ₆] ²⁺ system from the sp ^{1.04} MO donor at water molecule site to the isotropic AO acceptor at Ca(II) ion site (the outermost contours were plotted at contour 0.002 e.Bohr ⁻³). (b) Schematics of the relation of the rigidity to the ion-water bonding type. Two sketches of molecular bonding between the sp hybrid MOs paired with s-type AO (top site) and d-type AO (bottom site) including their hypothetical barrier results.	...	54
4.5. Water rotational rigidity energies for Ca[(H ₂ O) ₆] ²⁺ , Na[(H ₂ O) ₆] ⁺ and Fe[(H ₂ O) ₆] ²⁺	55
4.6. Contributions of non-interacting kinetic energies E_K and the others to the rotational rigidity energies as function of the rotational angle for Ca[(H ₂ O) ₆] ²⁺ and Fe[(H ₂ O) ₆] ²⁺ . We note that the ordinate denotes values measured from the total energy for the equilibrium structure.	...	56
Chapter V		
5.1. Structure model of [M(H ₂ O) ₆] ³⁺ systems as the initial structure		

for single water molecule dehydration.	...	59
5.2. (a) (leftmost) charge density distribution of Cr^{3+} , (right) the unpaired d -orbital distributions of Cr^{3+} ; (b) (leftmost) charge density distribution of Cr^{3+} , (right) the unpaired d -orbital distributions of Cr^{3+} ; (c) (leftmost) charge density distribution of Cr^{3+} , (right) the unpaired d -orbital distributions of Cr^{3+} ; (d) charge density distribution of Cr^{3+} and its spin configuration; (e) charge density distribution of Cr^{3+} and its spin configurationa) Average M-O distances, and (b) relative vibrational frequencies for symmetrical M-O stretching mode.	...	65
5.3. (upper) MOs energy and DOS equivalence for $[\text{Cr}(\text{H}_2\text{O})_6]^{3+}$ and $[\text{Fe}(\text{H}_2\text{O})_6]^{3+}$ systems, (bottom) fine-scale resolution of focused MO energies in $[\text{Cr}(\text{H}_2\text{O})_6]^{3+}$ system, two alpha MOs (inset figure) in group of $3a_1$ band at electron contour 0.03e/a.u. ³	66
5.4. Electronic interactions between Mn^{3+} and $6(\text{H}_2\text{O})$ MOs energies and DOS equivalence of $[\text{Mn}(\text{H}_2\text{O})_6]^{3+}$ system.	...	67
5.5. (a) Average M-O distances, and (b) relative vibrational frequencies for symmetrical M-O stretching mode.	...	68
5.6. (a) Average optimized OH distances, and (b) $\angle\text{HOH}$ angles of $[\text{M}(\text{H}_2\text{O})_6]^{3+}$ systems.	...	69
5.7. Relative potential energy curves (fully relaxed structure) of $[\text{M}(\text{H}_2\text{O})_6]^{3+}$ systems ($\text{M}=\text{Cr}, \text{Mn}, \text{Fe}, \text{Co}, \text{Ni}$, and Al) which M-O distances are used as constraint variables. The dehydration steps are symbolized by circled numbers. The symbols of $\text{Mn}(\text{x})$ and $\text{Mn}(\text{z})$ in figure legend stand for single dehydrations for $\text{Mn}(\text{III})$ -water cluster at x and z axes directions, respectively	...	70
5.8. The three PEC calculations of $[\text{Cr}(\text{H}_2\text{O})_5]^{3+}$, $[\text{Mn}(\text{H}_2\text{O})_5]^{3+}$, dan $[\text{Fe}(\text{H}_2\text{O})_5]^{3+}$ systems on water rotational rigidities.	...	71
5.9. Total dipole moments scanning for $[\text{Fe}(\text{H}_2\text{O})_6]^{3+}$ and $[\text{Cr}(\text{H}_2\text{O})_6]^{3+}$ systems.	...	72
5.10. The MOs energy and DOS equivalence of $[\text{Co}(\text{H}_2\text{O})_6]^{3+}$ system. Inset figure provides polar hybridized MOs at electron contour 0.03e/a.u. ³	73

List of Tables

	pg
Chapter II	
2.1. Average charge-transfer from monomer to others (CT_{AV}), average charge-transfer within monomer/isolated (NCT_{AV}) and average binding energies ($\Delta\overline{E}_b$) in dimer and cyclic trimer within the cyclization reaction from dimer to trimer of water clusters. Schematics of the initial and final states of the reaction are also shown. “stg” (surrounded by dashed curves) and “ecl” (surrounded by real curve) denote staggered binding character and eclipsed binding character, respectively. f^- and f^+ denote reactivity indices from Fukui functions.	... 28
Chapter III	
3.1. Averages and ranges of H-O distances in the pure water clusters. The experimental value for the bulk is also shown for reference.	... 40
3.2. The number of H-bonding, the average of H-bonding distances and H-bonding strengths from calculated cyclic, book and cage hexamer clusters. Here, H-O distance is the closest distances from H atom in one water molecule to O atom of one another, and H-bond strength is the average binding energy per H-bonding.	... 42
Chapter IV	
4.1. Ionization strengths from the first and second layers of Na(I), Ca(II), and Fe(II) aqueous clusters at 0 K and 353.15 K (1.0 atm).	... 50
4.2. Volume expansion indices V_x , the indices of internal pressure estimation X_c (KCal/cm ³) induced by a cation addition, and their qualitative statuses for Na(I), Ca(II), and Fe(II) aqueous clusters.	... 52
Chapter V	...
5.1. Absolute hardness for some monoatomic cations.	... 61
5.2. Properties of $[M(H_2O)_6]^{3+}$ systems obtained by the calculations	

	together with experimental hydration enthalpies per molecule as references.	...	64
5.3	Calculated M-O distances of $[M(H_2O)_6]^{3+}$ systems projected onto x, y, and z axes and related experimental data.	...	68

List of Selected Equations

	pg
Chapter II	
2.2. Kohn-Sham (KS)	... 16
2.4. Electrostatic potential	... 17
2.14. Fukui indices approximation	... 19
Chapter III	
3.2. Atomic force	... 33
3.3. Hessian	... 33
3.7. G constraint	... 35
3.8. BFGS algorithm	... 35
Chapter IV	
4.1. Ionization strength	... 45
4.4. Intermolecular binding energy	... 46
4.5. Volume expansion	... 46
4.7. Water rotational rigidity	... 47
Chapter V	
5.3. Classical electrostatic formulation	... 60
5.4. Hydration enthalpy	... 60
5.5. Dehydration reaction	... 61

Chapter I

Introduction

1.1 Background

Small water cluster systems have been largely studied for many years in the last decade since their potential applications are still growing up. Water clusters are involved in various areas of great scientific and technological importance, in atmospheric planetary, environment, biochemistry, and novel energy devices such as in the membrane design of Nafion-based Proton Exchange Membrane for Fuel Cell (PEMFC) [1] applications. The number of water molecules content inside the membrane is extremely small around 2-22 molecules. It is why experimentally studies on this water behaviour are arduous. The PEMFC is also one of the recent researches of the fuel cell technologies of which the significance is appreciated in Japan and some developed countries, for example, on the development of alternative catalysts to platinum [2–7] and the solution to the membrane degradation problem [8–12]. Membranes have a principal function of conducting protons from the anode to the cathode. The water content [8-9] of the PEM (Proton Exchange Membrane) [10] (electrolyte) has become one of the important subjects of investigation for preventing the membrane function debasement [11]. Systematic studies on small water started with pure water systems and then cationic water behaviours are expected to help for solving some membrane problems.

Theoretical study on small water systems will lead also to our understanding about some physical phenomena and chemical reactions. By this study, we may have information about intermolecular binding energy, monomer dipole moments, water formation and clustering, volume expansion, water rotational rigidity behaviour, etc. Such information is not only strongly related to the wet and dry condition of the membrane but also influencing proton transport through the membrane. Similarly, we may obtain some of chemical reactions, for instance: hydration reaction, forming enthalpy, single water dehydration reaction that they are related and supporting the

intermediate reaction of cationic attack at electrolyte polymer (such as polymer membranes).

In this study we select some interesting topics, those are, small water formation (chapter II) and stability (chapter III), cationic water behaviour (chapter IV), and single water dehydration at cationic water system (chapter V). Since the physical phase state of water may be determined by their intermolecular bond strength which possibly probed by monomer dipole moment quantity, and wet/dry condition of fuel cell polymer membrane can be estimated through the small number of water content behaviour inside the membrane, then the topic on clustering water (formation) and their stability, hopefully, will enlighten the membrane condition.

It is well known that the movement of a proton with alien cationic ions directly affects the water flux and proton conductivity of membranes, causing membrane degradation [12]. Na(I) and Ca(II) ions originally contained in Nafion membranes as contaminants may go into the water and consequently accelerate the degradation [12]. Nevertheless, a comparative study of very low concentration ions has shown that Ca(II) does not only improve the water content or resolve kinetic current degradation problems as compared with the Na(I), but it also has a more competitive mass density [13] (volume contraction effect). Theoretical investigations on the effects of adding Na(I) and Ca(II) ions to a small water cluster system, especially in order to address its advantages in PEMFC applications, are still rare and therefore this cationic water topic is desired.

The dehydration has been acknowledged as an essential molecular interaction for water-ion exchange reaction, since some experimental evidences have shown that ion attack at surfactants and polyelectrolyte is followed by its partial interaction of the counter-ions (dehydrated ion) [14-15]. A recent study on counter ion-binding (aqueous Al(III) and Cr(III)) related to the ion attack at electrolyte polyvinyl sulphate (PVS) has brought up that hydration enthalpy from coordinated water release within the primary hydration sphere plays a key role in driving binding to PVS [16]. Similar reactions possibly happen in a humid membrane of fuel cell, when contained water is starting dehydrated at working temperature. The residues of dehydrated cations [17] (e.g. Al(III) and Fe(III)) may attack and deactivate the proton hopping supports in the membrane (SO_3^- end). Such interaction can impair the functionality of membranes through protons

migration. The binding of first water layer with central cation is the strongest among the other water layers. Therefore, a single water dehydration topic at first water layer is observed in this study.

1.2 Problem

During study we have found and listed some problems as following:

- The formations of water clusters have many possible conformations or local minima [18-19] due to their weak intermolecular H-bonding. Thus, finding the most stable formations as hydration products could be arduous, and they strongly depend on the initial orientations of the clusters.
- Because the movement of a proton with alien cationic ions directly affects the water flux and proton conductivity of membranes, causing membrane degradation, a theory for the evaluation of the cationic effects of some cations (Ca(II), Na(I), or Fe(II)) addition to water is demanded.
- It has been stated that hydration enthalpy of $M[(H_2O)_6]^{3+}$ clusters with M=central metal ions influences the amount of reaction product in water and ion exchange reactions, nevertheless, theoretically, the activation energy should be more significant on determining the success of a reaction. Such clarification is needed to elucidate the dehydration mechanism and cationic effect in which they strongly affect to ion attack at electrolyte polymer. The activation energy may also determine amount of dehydration products which are reckoned in the enthalpy calculations.

1.3 Objective

The objectives of study are:

- to find a reliable theoretical approach in order to design the initial orientation for intermolecular formation, to analyse the local binding energy fluctuations in terms of the number of molecules and to observe the behaviour trend of the average binding energies for different cluster sizes, and to examine the water clusters physical state (phase) via their monomer dipole moments values with regard to the experimental values [20–22];

- to proposed a theory for the evaluation of the cationic effects of Ca(II), Na(I), or Fe(II) addition to water by first-principles calculations based on the density functional theory;
- to clarify that the activation energies of the dehydration reactions should be relevant to water and ion exchange reactions, particularly for exemplified metal ion attack at polyelectrolyte.

1.4 Methodology

The methodologies of studies are listed as following:

- the formations of small water systems will be obtained by constant adding one by one water molecule from monomer to the cluster systems (hydration reactions). A new method based on reactivity indices from Fukui functions has been introduced to generate the initial structures. The average binding energy and monomer dipole moment quantities will be used to get the cluster binding trend and wet/dry condition of cluster;
- the cationic effects of Ca(II), Na(I), or Fe(II) addition to water will be evaluated by proposing definitions of index parameters for the ionization strength, volume expansion, and water rotational rigidity (at small rotational angles) of cationic aqueous systems;
- the single water dehydration mechanism (dissociation processes) of hydrated metal ions will be computed where the M-O distances were chosen as the constraint variables, while the other inter-atomic distances had been fully relaxed.

1.5 Scope

The cations as the water impurities in this study are only limited for Na(II), Ca(II), Fe(II), Cr(III), Mn(III), Fe(III), Co(III), Ni(III) and Al(III). Number of water molecules is confined from 1 to 18 molecules (up to two layers water in case of cationic water systems).

1.6 Systematic

We have arranged the contents of thesis into six chapters including:

Chapter I Introduction

Chapter II	The Formation of Small Water Cluster Systems
Chapter III	The Stability of Small Water Cluster Systems
Chapter IV	Small Water Clusters Role in Fuel Cell Membrane
Chapter V	Single Water Dissociation Effect in Ion-exchange Reaction
Chapter VI	Conclusions

Chapter II

The Formation of Small Water Cluster Systems

2.1. Introduction to DFT

The idea of density functional theory (DFT) originally comes from Thomas-Fermi (TF) theory (1920) that it forms a relation between total electronic kinetic energy with electron density functional, expressed as:

$$T_{TF}[\rho] = C_F \int \rho^{5/3}(\vec{r}) d\vec{r}, \quad C_F = \frac{3}{10} (3\pi^2)^{2/3}. \quad (2.1)$$

T_{TF} , ρ and C_F are represented total electron kinetic energy based on Thomas-Fermi theory, electron density and Fermi constant, respectively.

By correcting kinetic energy into exchange-correlation functional, Thomas-Fermi theory had been successfully expanded to Kohn-Sham method (1960) which is also known as DFT [47]. A Kohn-Sham (KS) method generates the fictitious system of non-interacting electrons which their density equal to the density of the interacting electrons. In principle, KS method work based on the following KS equations:

$$\left[-\frac{1}{2} \nabla^2 + v_{eff}(\vec{r}) \right] \psi_i = \varepsilon_i \psi_i \quad (2.2)$$

which

$$v_{eff}(\vec{r}) = v(\vec{r}) + \frac{\delta J[\rho]}{\delta \rho(\vec{r})} + \frac{\delta E_{xc}[\rho]}{\delta \rho(\vec{r})}$$

and total electron density $\rho(\vec{r}) = \sum_i^N \sum_s |\psi_i(\vec{r}, s)|^2$.

The functional energies v_{eff} , v , J , and E_{xc} are respectively represented KS effective potential, external potential, Coulomb energy, and exchange-correlation energy.

Variational principle state that total electronic energy computed from guessed wave function ψ_i is upper bound to the ground state energy E_g , expressed by:

$$E_g(\psi_0) = \min_{\psi} [E(\psi)]. \quad (2.3)$$

Then, latest equations must be solved self-consistently that are using self-consistent field (SCF) procedure.

Once the KS equations are solved, we may obtain information about the ground state energy ($E_g(\psi_0)$) relative orbital energies (ϵ_i), total electron density ($\rho(\vec{r})$) and orbital distribution of observed system ($\psi_i(\vec{r}, s)^2$).

2.2. Molecular active site

Electrostatic potential and Fukui indices are essential properties for approximating site reactivity in the intermolecular binding and reaction. The derivations for both properties are coming from the DFT which some of them already have discussed.

2.2.1. Electrostatic potential

Molecular electrostatic potential (MEP) are usually calculated by theoretical for getting insight into the structure and reactivity of molecules. The MEP, $V(r)$, generated due to of N nuclei with charges Z_A and located R_A and corresponding continuous electron density is given by:

$$V(\vec{r}) = \sum_A \frac{Z_A}{\|\vec{r} - \vec{R}_A\|} - \sum_{\mu} P_{\mu\nu} \int \frac{\phi_{\mu}(\vec{r}') \phi_{\nu}^*(\vec{r}') d\vec{r}'}{\|\vec{r} - \vec{r}'\|} \quad (2.4)$$

which $P_{\mu\nu}$ represents the density matrix.

Commonly, for molecular systems dominantly contain an ionic character.

2.2.2. Fukui indices

Before we derive Fukui indices let consider the differential expression for the change from one ground state to another for some electronic system energy $E=E[N, v]$:

$$dE = \left(\frac{\partial E}{\partial N} \right)_v dN + \int \left[\frac{\delta E}{\delta v(r)} \right]_N dv(r) dr \quad (2.5)$$

This equation can be written in term of ρ as in $E=E[\rho]$:

$$dE = \int \left[\frac{\delta E}{\delta \rho(r)} \right] d\rho(r) dr + \int \left[\frac{\delta E}{\delta v(r)} \right]_{\rho} dv(r) dr \quad (2.6)$$

The ground state $\rho(r)$ must satisfy the Euler equation described in first subtitle and expressed as:

$$\left[\frac{\delta E}{\delta \rho(r)} \right]_{\nu} = \mu = \text{const.} \quad (2.7)$$

While from first perturbation formula $E^{(1)} = \langle \Psi^{(0)} | \Delta V | \Psi^{(0)} \rangle$ we obtain:

$$E = \rho(r) \Delta v(r) dr \quad \text{or} \quad \left[\frac{\delta E}{\delta v(r)} \right]_{\rho} = \left[\frac{\delta E}{\delta v(r)} \right]_N = \rho(r) \quad (2.8)$$

Finally we satisfy differential energy of the change from one ground state to another as:

$$dE = \mu dN + \int \rho(r) dv(r) dr \quad (2.9)$$

Similarly, considering $dN = \int \rho(r) dr$ then $\mu = (\partial E / \partial N)_{\nu}$, the differential chemical potential ($d\mu$) can be derived as:

$$d\mu = \left[\frac{\partial \mu}{\partial N} \right]_{\nu} dN + \int \left[\frac{\delta \mu}{\delta v(r)} \right] dv(r) dr \quad (2.10)$$

To simplify this expression we introduce symbol η (hardness) and f (Fukui function):

$$2\eta = \left(\frac{\partial \mu}{\partial N} \right)_{\nu} \quad \text{and} \quad f(r) = \left(\frac{\delta \mu}{\delta v(r)} \right)_N \quad (2.11)$$

Then we obtain:

$$d\mu = 2\eta dN + \int f(r)dv(r)dr \quad (2.12)$$

The physical meaning of $f(r)$ is implied by its definition as $[\delta\mu/\delta(r)]_N$: it measures how sensitive a system's chemical potential is to external perturbation at a particular point.

By recalling Maxwell relation, the relation manifests Fukui function from chemical potential and external energy to kernel/orbital electron density terminology:

$$f(r) = \left(\frac{\delta\mu}{\delta v(r)} \right)_N = \left(\frac{\partial \rho(r)}{\partial N} \right)_v \quad (2.13)$$

Suppose we are in going from N electrons to $N+\delta$ electrons, consequently we have three indices:

$$f^+(r) = \left(\frac{\partial \rho(r)}{\partial N} \right)_v^+ \quad (\text{derivative as } N \text{ increase from } N_0 \text{ to } N+\delta)$$

$$f^-(r) = \left(\frac{\partial \rho(r)}{\partial N} \right)_v^- \quad (\text{derivative as } N \text{ increase from } N_0 \text{ to } N-\delta)$$

$$f^0(r) = \frac{1}{2} [f^+(r) + f^-(r)] \quad (\text{mean of left and right derivative})$$

with approximate formula:

$$f^+(r) \approx \rho_{LUMO}(r), f^-(r) \approx \rho_{HOMO}(r) \text{ and } f^0(r) = 0.5 \times (\rho_{LUMO} + \rho_{HOMO}) \quad (2.14)$$

These indices can measure the preferences for a site of reagent one kind or another:

$f^+(r) \rightarrow$ measures a reactivity toward a nucleophilic reagent

$f^-(r) \rightarrow$ measures a reactivity toward an electrophilic reagent

$f^0(r) \rightarrow$ measures a reactivity toward a radical reagent

based in these site reactivity, the fukui indices known as natural index reactivity. The reactivity index can be used to prepare a good initial structure and act as the fundamental approximation for frontier orbital.

2.3. Atomic charge and monomer dipole moment

With DFT result obtained on the charge distribution, it is now possible to observe interatomic interactions (for instance charge transfer, dipole moment, etc.) by considering electrons condensed to nuclei (as point of charge approximation). Some electron population methods had been proposed for this approximation, for example Mulliken population analysis (MPA), Bader population analysis (AIM), natural population analysis (NPA), restrain electrostatic potential (RESP), etc.

In computational, we may rewrite total electron density in density matrix (P) and orbital basis (ϕ) term, as following

$$\rho(\vec{r}) = \sum_{\mu\nu} P_{\mu\nu} \phi_{\mu}(\vec{r}) \phi_{\nu}^*(\vec{r}) \quad (2.15)$$

$$P_{\mu\nu} = 2 \sum_i^{N/2} C_{\mu i} C_{\nu i}^* = P \quad (2.16)$$

where C represents expansion coefficients, and then overlap matrix can also be expressed as:

$$S_{\mu\nu} = \int d\vec{r}_A \phi_{\mu}^* \phi_{\nu} = S \quad (2.17)$$

The MPA is based on a half of total orbital overlap put through summation of nuclei charge, local charge (diagonal density matrix $Tr(P)$), and half of overlap population (off-diagonal part) [25]

$$q_A = Z_A - \sum_{\mu \in A} (PS)_{\mu\mu} \quad (2.18)$$

which may be suitable for covalent bonds (σ) but insufficient for evaluating double bonds (π) and non-covalent bonds.

The disadvantage of MPA on the π bond type of orbital evaluation has been attempted to recover by the atom in molecule (AIM) population method. The method utilizes Laplacian of the total electron density (L)

$$L(\vec{r}) = -\left(\frac{\hbar^2}{4m}\right) \nabla^2 \rho(\vec{r}) \quad (2.19)$$

that its integral over an atom A to yield $L(A)$

$$\begin{aligned} L(A) &= \int_A -\left(\frac{\hbar^2}{4m}\right) \nabla^2 \rho(\vec{r}) d\tau \\ &= \left(-\frac{\hbar^2}{4m}\right) \oint dS(A, \vec{r}) \nabla \rho(\vec{r}) \cdot \vec{n}(\vec{r}) = 0 \end{aligned} \quad (2.20)$$

vanish the zero flux boundary condition which defines an atom in a molecule. The AIM method or Bader analysis has generally implemented electron contour topology at bond region (bond critical point or BCP) for total electron which able to cover all covalent interaction including the π bond.

However, both previous methods tend to follow a concept of ‘electrons condensed to nuclei’ rather than a central ‘point of charge’ method. A charge analysis centred on nuclei which was previously proposed for high ionic character based on occupancies of the orthonormal natural atomic orbitals, that is the natural population analysis (NPA), had exhibited a better performance than the MPA, and somehow, in case of systems having ionic character, it had also shown a more accurate result than the AIM one. Basically, the concept of natural orbital follows previous Löwdin population that transform density matrix P into P' . Let’s start again with number of electron (two electrons per molecular orbital)

$$N = \sum_{\mu} \sum_{\nu} P_{\mu\nu} S_{\nu\mu} = \sum_{\mu} (PS)_{\mu\mu} = \text{tr} PS \quad (2.21)$$

Because $\text{tr} PS = \text{tr} SP$, then we may rewrite

$$N = \sum_{\mu} (S^{\alpha} P S^{1-\alpha})_{\mu\mu} \quad (2.22)$$

and with $\alpha = \frac{1}{2}$, then the equation become

$$N = \sum_{\mu} (S^{1/2} P S^{1/2})_{\mu\mu} = \sum_{\mu} P'_{\mu\mu} \quad (2.23)$$

Using similar MPA equation we now have another (natural) atomic charge population

$$q_A = Z_A - \sum_{\mu \in A} (P')_{\mu\mu} \quad (2.24)$$

which P' is the density matrix in term of a symmetrically orthogonalized basis set,

$$\rho(\vec{r}) = \sum_{\mu} \sum_{\nu} P'_{\mu\nu} \phi'_{\mu}(\vec{r}) \phi'_{\nu}^*(\vec{r}) \quad (2.25)$$

$$\phi'_{\mu}(\vec{r}) = \sum_{\nu} (S^{-1/2})_{\nu\mu} \phi_{\nu}(\vec{r}) \quad (2.26)$$

Further transformation development had been discussed by Weinhold, F. et al. [26]. Nevertheless, the NPA still utilizes transformed orbitals (indirect) calculation which may has accumulation distortion.

Unlike NPA, The RESP analysis is underlying on electrostatic potentials to derive atomic charges represents a common least-squares fit of criterion

$$R = \sum_i^m w_i \left[V_i^0 - \sum_A^{n-1} q_A r_{iA}^{-1} + \left(\sum_A^{n-1} q_A \right) r_{in}^{-1} - Z r_{in}^{-1} \right]^2 \quad (2.27)$$

where V_i^0 represents computed electrostatic potential at point i , q_A is the net charge on atom A , r_{iA} is the distance between atom A and the i -th grid point, m is the number of grid point, n is the number of atoms, and Z represents the net charge on the molecule, which is equal to zero for non-ionic species. Remaining two terms of R reflect the condition that the net atomic charge must sum to Z . And, to minimize value of R , the first partial derivative of R with respect to each of the $(n-1)$ independent net atomic charge were acquired; therefore the resulting linear equations can be solved by usual least square technique.

The other essential property of small water cluster systems is the monomer dipole moment. Experimentally [27], one way to distinguish whether water in gas, liquid or ice phase, is measured by the monomer dipole moment property. The dashed line in Figure 2.1 shows the monomer dipole moments level for gas phase water is around 1.855 Debye, for the liquid phase is around 2.45 Debye and for solid phase is around 2.6 Debye. The monomer dipole moments have been calculated using Eq. (2.28) and fitted by dipole moment value of gaseous water.

$$\mu = 4.803 \times \frac{\sum_{i=1}^n \sqrt{(q_i^{\text{APT}} d_{ix})^2 + (q_i^{\text{APT}} d_{iy})^2 + (q_i^{\text{APT}} d_{iz})^2}}{n} \quad (2.28)$$

where sup script APT denote atomic polar tensor population.

Based on these properties, the tetramer, pentamer, and hexamer are close to the solid phase. However, the cage hexamer is supposed to be the smallest stable liquid formation. The heptamer is close to liquid phase and others higher number of molecules are in the transition between the liquid and solid phase. For dimer and trimer, their phases are in the transition between gas phase and liquid phase. Experimentally [27], the monomer dipole moment can be approximated by calculating second order perturbation energy of Stark effect. These studies implement an electric field to the cluster system, which it will polarizes each cluster monomer. Then after the electric field was removed, the value of monomer dipole moment should be proportional to the second-order Stark energy.

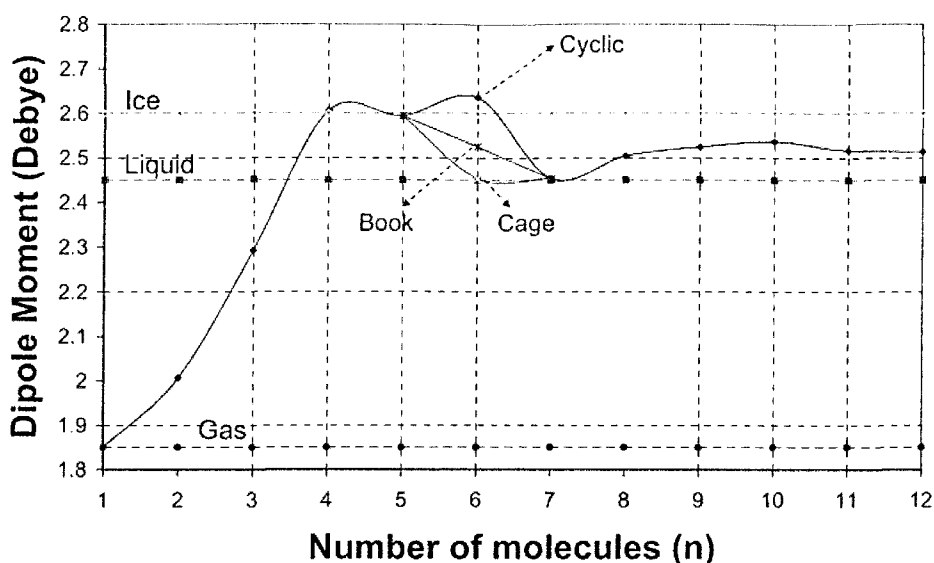


Figure 2.1 The monomer dipole moments of small water cluster with $n = 1$ to 8. The dashed lines in main figure are taken from experimental data [28–30] for gas, liquid and solid phase. These studies have used atomic polar tensor (APT) charge in order to calculate the monomer dipole moment values.

2.4. A case study on small water clusters formation

Recently, the performance of PEMFC is highly expected to be affected by the clustering behavior of water molecules at the molecular level, which control the humidity conditions (wet/dry) inside the Nafion [32, 33] membrane.

Wet and dry conditions are strongly related to the physical phase states of matters. In case of very small water cluster systems, it is still hard to identify the phase state of the clusters. A systematic scheme is needed to identify the structures (formation) stabilities, to analyze the intermolecular binding energy trend, and to evaluate the molecular dipole moment values. From our preliminary study, we have investigated the most stable formations and the average binding energies trend of small water clusters as the number of molecules are increased using the density functional theory (DFT). The formation of water clusters has many possible conformations or local minima [34-35] due to their weak intermolecular H-bonding. Thus, finding the most stable formations as hydration products could be arduous, and they strongly depend on the initial

orientations of the clusters. One of physical properties that make sense to distinguish between the liquid and solid phase in condensed matter is the stability of structures which are associated with the intermolecular binding energies. However, the property has no charge distribution information. Other identifying of the phase state which include the atomic charge distribution information had been made experimentally by measuring the monomer dipole moments (dipole moment is a vector) of bulk water system [36–38]. But it is still uneasy to obtain experimentally the properties on small scale of water cluster systems. Since the hydration reactions also have wide spread applications in chemistry, we have separated our investigation purposes into some objectives.

There are three objectives to be achieved for these studies; the first one is to find a reliable theoretical approach in order to design the initial orientation for intermolecular formation. This could be solved by determining the reactivity index to reduce search of the number of reactive sites between the host cluster and the guest single water molecule in the molecule reactions (hydrations). The second one is to analyse the local binding energy fluctuations in terms of the number of molecules and to observe the behaviour trend of the average binding energies for different cluster sizes. The last one is to examine the water clusters physical state (phase) via their monomer dipole moments values with regard to the experimental values [36–38].

A systematic scheme has been used. We have employed a DFT approach using different basis set based on B3LYP (Becke-3 parameters-Lee-Yang-Parr) exchange correlation functional [39] and 6-311++G(2d,2p) [40] to optimize the cluster geometry. One of the reasons in utilizing this functional is that the three parameters of B3LYP had been fitted to gaseous water data, better than unfitted BLYP (GGA type).

The reactivity index from Fukui functions [41] have been used to predict the initial structures of the clusters. The basic idea of this prediction is that the chemical potential (μ) differences drive the electron transfer from one system to another. Because the physical meaning of Fukui functions $f(r)$ is implied by its definition as functional derivative $[\delta\mu/\delta(r)]_N$: it measures how sensitive a system's chemical potential is to external perturbation at a particular point, then the overlap of left $f^-(r)$ and right $f^+(r)$

derivative (reactivity indices) will give us prediction directions for the initial structures with more charge-transfer indicating a stable structures approximation. In these studies, the f^- and f^+ reactivity indices have been approached using isosurfaces of the Highest Occupied Molecular Orbitals (HOMOs) and the Lowest Unoccupied Molecular Orbitals (LUMOs).

Calculated charge-transfer populations was estimated using natural bond orbital [42] (NBO) have been also considered to evaluate the trimer ($n=3$) binding characters. A saddle point optimizations are also performed to get the activation energy of hexamers in order to complete their stabilities analysis. The average binding energies and local binding energies are determined by the following equation:

$$\Delta\bar{E}_b = \frac{E((H_2O)_n) - nE(H_2O)}{n}, \quad (2.29)$$

$$\Delta E_h = E((H_2O)_n) - E((H_2O)_{n-1}) + E(H_2O), \quad (2.30)$$

where $\Delta\bar{E}_b$, ΔE_h , $E((H_2O)_n)$, $E(H_2O)$, and n denote the average binding energy, the absolute (hydration) binding energy when a H_2O approaches $(H_2O)_{n-1}$ cluster, the total energy of cluster system, the total energy of isolated water molecule, and number of molecules, respectively.

Equation (2.29) pertains to the average binding energy needed to dissociate or hydrate all water molecules from/to their cluster. Equation (2.30) represent the local binding energy needed (in equilibrium) to add or remove only one water molecule to or from the cluster. Both quantities refer to the intermolecular bond strength of the clusters. However, the average binding energies could have significant roles as the references for the fluctuations of the first equation and also their trend will lead to the average intermolecular binding energy of ice water.

The overestimated bond strength of $1b_2$ molecular orbital (MO) in the dimer ($n = 2$) can be reduced by adding more d functions to O atoms and more p functions to H atoms in basis set modifications [43].

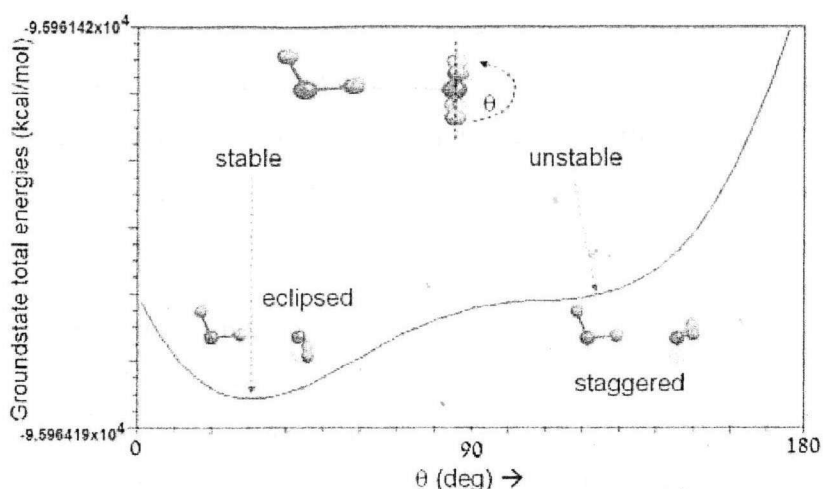


Figure 2.2 The stability of eclipsed dimer is examined by scanning the energy profile as the H atoms are rotated (θ) from 0° to 180° with O atom as the center of rotation.

The obtained functions for O atoms and H atoms will strengthen the covalent characters and reduce the overestimated orbital bond strength indicated by means of the intermolecular binding. The B3LYP has been chosen in order to consider that both the non-correlation model (Hartree Fock) [44] and the smaller correlation parameter model (BLYP) could not give higher intermolecular binding. In addition, we also compare the results from HF and BLYP models, and we obtain a lower binding energy using B3LYP in optimized dimer which shows a good agreement with experimental values [45]. The monomer dipole moments are calculated by point of charge approximation that taking account Atomic Polar Tensor (APT) population analysis (the APT charge was obtained from G03 software [46]) which is condensed in atomic charge. To be different from Mulliken population analysis, APT population is based on the electron distribution (electron density) in molecules that is not distorted by an arbitrary choice of the reference basis set as reported by Cioslowski [47] (one of Gaussian03 contributors). The grid of numerical integration is pruned (75,302) grid, having 75 radial shells and 302 angular points per shell. The monomer dipole moments using APT population can be represented by following equation:

$$\mu = 4.803 \times \frac{\sum_{i=1}^n \sqrt{(q_i d_{ix})^2 + (q_i d_{iy})^2 + (q_i d_{iz})^2}}{n} \quad (2.31)$$

where μ , q , d , and n denote monomer dipole moment (in Debye), atomic charge (APT population) (in e), atomic position (in Angstrom), and number of molecules, respectively, and x , y , z are coordinates (projected positions).

Table 2.1 Average charge-transfer from monomer to others (CT_{AV}), average charge-transfer within monomer/isolated (NCT_{AV}) and average binding energies ($\Delta\bar{E}_b$) in dimer and cyclic trimer within the cyclization reaction from dimer to trimer of water clusters. Schematics of the initial and final states of the reaction are also shown. “stg” (surrounded by dashed curves) and “ecl” (surrounded by real curve) denote staggered binding character and eclipsed binding character, respectively. f^+ and f^- denote reactivity indices from Fukui functions.

	Dimer	Cyclic trimer
CT_{AV}	0.0131 e	0.0158 e
NCT_{AV}	0.0081 e	0.0062 e
$\Delta\bar{E}_b$	-2.49 kcal/mol	-5.12 kcal/mol
	Initial structure	Final structure

(a)

(b)

A good initial prediction of the nano structures chemistry based on reactivity index from Fukui functions can be found in the stereo-selection of water dimer structures. In order to form a stable dimer structure, there are two logical approaches that a water molecule could take; one approach is where the planes of the water molecule are perpendicular to each other; and the other, the planes are in parallel.

In both cases, the O atom of the approaching molecule connects with H atom of the other molecule. For this reason, the former (eclipsed formation) will be more stable because H atoms are closer to the f^- Fukui functions (reactivity toward an electrophile reagent) than the latter (staggered). The stability of the eclipsed dimer has been also

examined with another dimer conformer by scanning the energy profile as the H atoms are rotated for about 180 degrees with O atom as the centre of rotation. The other conformer (staggered formation) is found on unstable valley curve (Figure 2.2). The maximum energy difference from this rotation is about 2 kcal/mol. It indicates that H-bonding energy has a relative wide-quality based on its structures. Here, we have found that the staggered structure is unstable and the eclipsed is the most stable configuration because the staggered structure has higher repulsive interaction between H atoms than the eclipsed one. Based from these structures, we state the binding tendencies of the molecules as staggered and eclipsed characters, as commonly used terminologies in chemistry.

The cyclization is essential in the small water cluster reactions, since the experimental results showed that clusters from 3 to 6 molecules are stable in the cyclic formations [48]. Using structure selections from the Fukui functions, the initial structure of cyclic trimer can be prepared well as shown at the dimer row in Table 2.1. (a). The figure at trimer row inside Table 2.1 (b) is the final structure of water trimer after optimization.

The preparation initial structures have shortened the optimization process, which means that the iterative steps are lesser and this will reduce the computational cost. Our calculations show that staggered binding character has a weaker H-bond and longer O-O distance as compared with the eclipsed ones, as summarized in Table 2.1. These results are also supported by the charge-transfer analysis. We have found that majority of the donor orbitals are from the lone pair orbitals or the HOMOs of each water molecule unit and majority of the acceptor orbitals are from the LUMOs of the other neighbor unit molecule. The figure (b) Table 2.1 shows that the amount of charge transferred to stagger formation is lesser than that of eclipse. With the similar ways, we also have prepared the initial structures for water tetramer ($n=4$, as shown in figure 2.3) and the others higher number of molecules based on the reactivity index from Fukui functions. The summary steps of the initial structure preparation based on the reactivity index are: (a) Calculating the f^- and f^+ isosurfaces of the host and guest system, (b) determining position of the biggest isosurfaces of the f^- and f^+ , (c) moving the guest molecule close

to the host system with respect to the great overlapping between the f^- and f^+ , and (d) if possible, avoiding both the f^- and f^- and also f^+ and f^+ isosurfaces meeting.

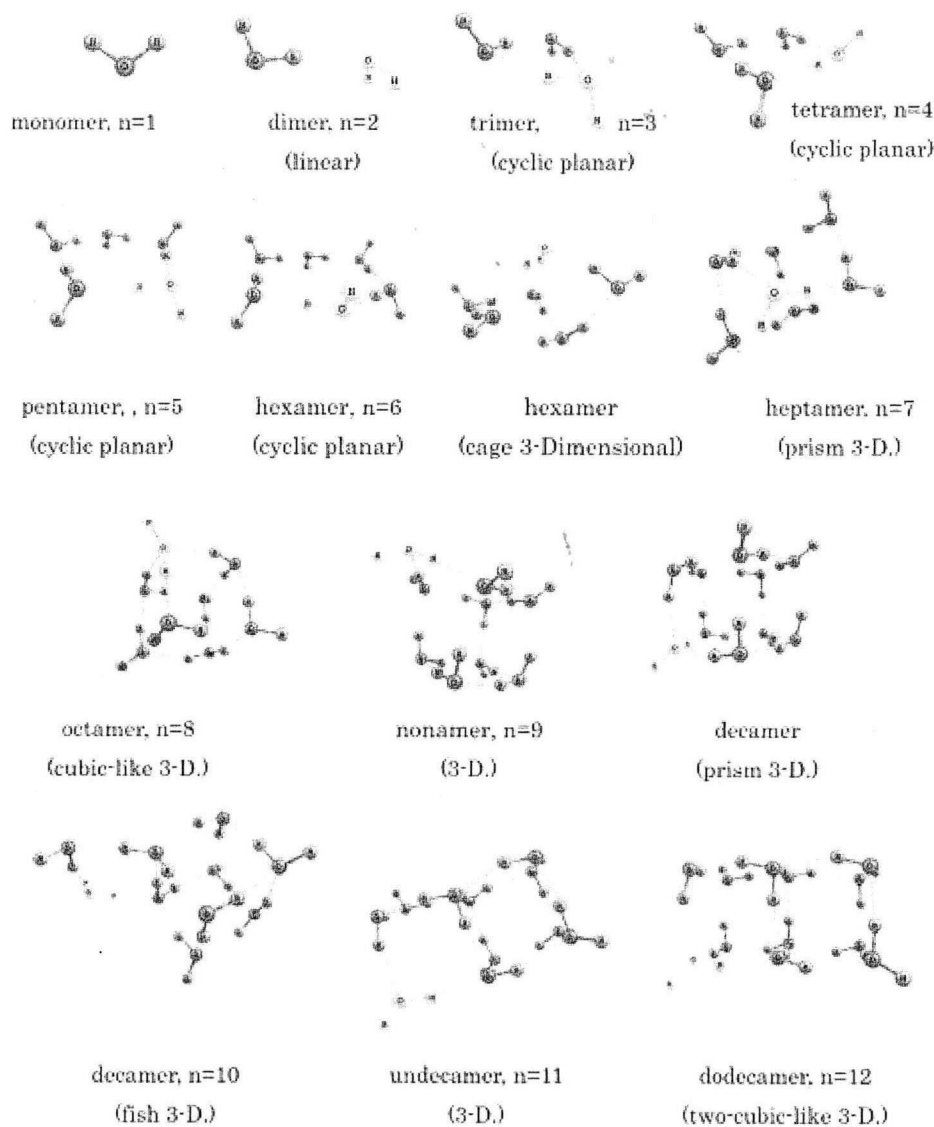


Figure 2.3 Water cluster formations are arranged from cluster structures with $n = 1-12$. The white color of water molecule is approaching molecule. The structures of hexamer ($n = 6$) and decamer ($n = 10$) are shown into 2 stable formations.

Figure 2.3 shows the optimized cluster structures from monomer ($n=1$) to dodecahomer ($n=12$) and Figure 2.4 manifests the average binding energies trend and local binding energies fluctuations. For higher number of clusters, it can be observed

that the former planar formations have been transformed to 3-dimensional formations. The shape transformation results also agreed with other theoretical studies that was shown based on stability energy, the cyclic hexamer was changed to prism34 [49]. However, the number of water molecules in that ref. [47] ($n=1-10$) is inadequate to predict the average binding energy trend with regard to the local fluctuation effects. For cyclic formations with $n=3$ and $n=4$, the additions of eclipsed and staggered characters stabilize significantly their binding energies. However, as the number of molecules increases ($n=5$ and $n=6$), the diameters of planar formations lengthen and as a consequence the inter-molecular separation is also increased; hence the values of average binding energies is decreased.

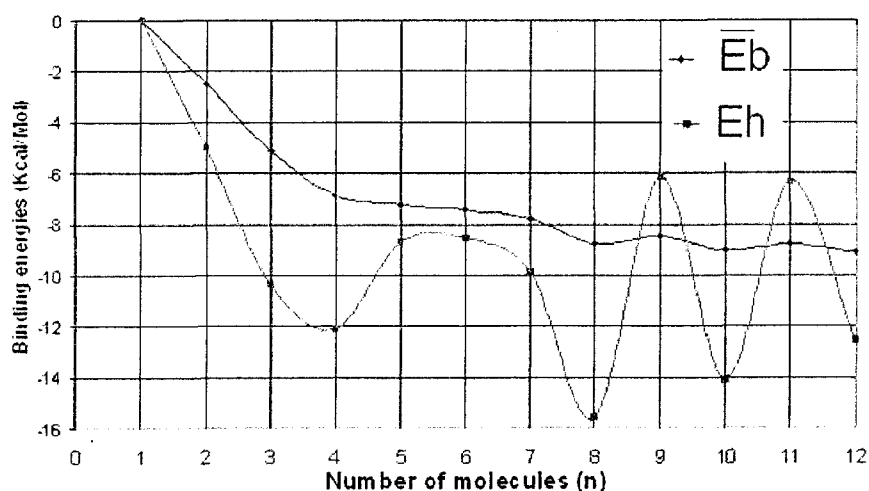


Figure 2.4 The average (ΔE_b) binding energies trend and local (ΔE_h) binding energy fluctuations for the most stable findings (linear dimer, cyclic planar trimer, cyclic planar tetramer, cyclic planar pentamer, cyclic planar hexamer, prism34 3-D. heptamer, cubic-like 3-D. octamer, prism45 3-D. nonamer, fish 3-D. decamer, asymmetric 3-D. undecamer, two-cubic-like 3-D. dodecamer) of small water cluster systems.

The symmetry (well-ordered) of the cluster is broken in heptamer ($n=7$) structures and the cyclic formation from hexamer does not expand, but instead to rearrange into 3-dimensional formation. The 3-D formation is continued in the optimized octamer ($n=8$) formation but its local binding energy has significantly decreased as

shown in Figure 2.4. It happens because besides having high symmetrical (ordered) structures, the cubic-like formation of the octamer could reduce the intermolecular separations. In case of the nonamer ($n=9$), the addition of one water molecule forms two H-bonds but breaks one of the other H-bond. It has responsibility for increasing the local binding energy. The decamer ($n=10$) has two most stable structures: prism and fish formations. Both formations have high ordered structures and tend to lower (stabilize) the local binding energy values. The prism-like formation of dodecamer ($n = 12$) looks like a two-layer cyclic hexamer structures but the two-cubic-like formation has the most stable one, as opposed to the previous hexamer stability examination. Our explanation is that the existences of additional four weak H-bonds at the middle of the two-cubic-like formation prohibit the two-layer book formation. Therefore, the higher symmetrical two-cubic like formation is favoured. From the observed fluctuations, it can be deduced that odd number of clusters have lower absolute binding energies than the even number ones. The fluctuation energies on higher number of molecules cannot be easily estimated from the local binding energy graph. However, we can predict the average binding energy trend (Figure 2.4) that for $n \geq 12$ tend to asymptotically converged at intermolecular average binding value of ice cluster. The reason is that, by constant increasing one molecule at a time would give smaller contribution at higher number of molecules. Then, the fluctuation effects on the average binding energies are reduced.

Although recent mathematical algorithm has offered some alternative scheme to obtain/approach the global minimum energy, however, the small water cluster formations (n water molecules) prepared by this study may benefit in lowering barrier energy from one formation to another formation since they preserves the previous formations ($n-1$ water molecules). In case of weak intermolecular interaction with dominated by correlation interaction, the initial structures prepared by Fukui indices (frontier orbital approximation) make a promise for stable bonding deduced by charge transfer mechanisms rather than that prepared by electrostatic potentials.

Chapter III

The Stability of Small Water Cluster Systems

We will introduce some optimization technique to obtain an optimized structure at ground state energy and transition structure at saddle point energy. The stabilities of molecular systems are dependent on the ground state and saddle point energy.

3.1. Introduction to molecular structure optimization

The energy E of molecular system is a parametric function of nuclear positions X_A . Let assume nuclei position move from X' to X , and the change of $\Delta X = X' - X$ will give $E(X') = E(X) + \Delta E$. Using Taylor expansion, one can obtain

$$E(X') = E(X) + \Delta X^\top f(X) + \frac{1}{2} \Delta X^\top H(X) \Delta X + \dots \quad (3.1)$$

where $f_i = \frac{\partial E(X)}{\partial X_i}$ and the Hessian $H_{ij} = \frac{\partial^2 E(X)}{\partial X_i \partial X_j}$

The derivation of f and H result in following equation:

$$\begin{aligned} \frac{\partial E}{\partial X_A} = & \sum_{\mu\nu} P_{\nu\mu} \frac{\partial H_{\mu\nu}^{core}}{\partial X_A} + \frac{1}{2} \sum_{\mu\nu\lambda\sigma} P_{\nu\mu} P_{\lambda\sigma} \frac{\partial(\mu\nu\|\sigma\lambda)}{\partial X_A} + \frac{\partial V_{NN}}{\partial X_A} \\ & + \sum_{\mu\nu} \frac{\partial P_{\nu\mu}}{\partial X_A} H_{\mu\nu}^{core} + \sum_{\mu\nu\lambda\sigma} \frac{\partial P_{\nu\mu}}{\partial X_A} P_{\lambda\sigma} (\mu\nu\|\sigma\lambda) \end{aligned} \quad (3.2)$$

and

$$\begin{aligned} \frac{\partial^2 E}{\partial X_A \partial X_B} = & \sum_{\mu\nu} P_{\nu\mu} \frac{\partial^2 H_{\mu\nu}^{core}}{\partial X_A \partial X_B} + \frac{1}{2} \sum_{\mu\nu\sigma\lambda} P_{\nu\mu} P_{\lambda\sigma} \frac{\partial^2(\mu\nu\|\sigma\lambda)}{\partial X_A \partial X_B} \\ & - \sum_{\mu\nu} Q_{\nu\mu} \frac{\partial^2 S_{\mu\nu}}{\partial X_A \partial X_B} + \frac{\partial^2 V_{NN}}{\partial X_A \partial X_B} + \sum_{\mu\nu} \frac{\partial P_{\nu\mu}}{\partial X_B} \frac{\partial H_{\mu\nu}^{core}}{\partial X_A} \\ & + \sum_{\mu\nu\sigma\lambda} P_{\nu\mu} \frac{\partial P_{\lambda\sigma}}{\partial X_B} \frac{\partial(\mu\nu\|\sigma\lambda)}{\partial X_A} - \sum_{\mu\nu} \frac{\partial Q_{\nu\mu}}{\partial X_B} \frac{\partial S_{\mu\nu}}{\partial X_A} \end{aligned} \quad (3.3)$$

where (in atomic unit)

$$(\mu\nu|\sigma\lambda) = (\mu\nu|\sigma\lambda) - \frac{1}{2}(\mu\lambda|\sigma\nu), \text{ two-electron interaction}$$

$$(\mu\nu|\sigma\lambda) = \int dr_1 dr_2 \phi_\mu^*(1) \phi_\nu(1) r_{12}^{-1} \phi_\sigma^*(2) \phi_\lambda(2)$$

$$H_{\mu\nu}^{core} = \int dr_1 \phi_\mu^*(1) h(1) \phi_\nu(1), \text{ one-electron interaction}$$

$$h(1) = -\frac{1}{2} \nabla_1^2 - \sum_A \frac{Z_A}{|r_1 - R_A|}, \text{ kinetic energy and attractive nuclei-electron potential}$$

$$S_{\mu\nu} = \int dr_1 \phi_\mu^*(1) \phi_\nu(1), \text{ overlap electron integral}$$

$$V_{NN} = \sum_{A=1}^M \sum_{B>A}^M \frac{Z_A Z_B}{R_{AB}}, \text{ repulsive inter-nuclear interaction}$$

$$Q_{\nu\mu} \equiv 2 \sum_a^{N/2} \varepsilon_a C_{\mu a} C_{\nu a}$$

The detail of derivation for (3.2) and (3.3) can be found in ref. [50].

Although the Taylor series is infinite, it can be approximated using only quadratic form: Let assume $X=X_e$ where $f(X_e)=0$ is the stationary point condition at X_e equilibrium positions. Thus, the next energy in term of the next position can be expressed as:

$$E(X_1) = E(X_e) + \frac{1}{2} \Delta X^\top H(X_e) \Delta X \quad (3.4)$$

In similar manner,

$$f(X_1) = f(X) + H(X) \Delta X \quad (3.5)$$

If the next positions also assume in equilibrium than $X_I=X_e$, and

$$f(X) = -H(X) \Delta X \quad \text{or} \quad \Delta X = -H^{-1}(X) f(X) \quad (3.6)$$

Now, position changes can be obtained by updating the gradient and Hessian values.

Some optimization algorithms are needed that the procedure might then repeated until:

$E_n - E_{n-1}$ is below a given threshold, $\sigma = f(X_n)^\top f(X_n)$ is below the threshold, $\Delta X^\top \Delta X$ is below a given threshold, or all three.

Let define constraints G , as following:

$$G\Delta X_n \equiv H^{-1}\Delta f_n = \Delta X_n \quad (3.7)$$

where $\Delta f_n = f_n - f_{n-1}$

The most successful algorithm for quantum engineer appears to be the BFGS method [51], defined by:

$$G_n = \left(1 - \frac{\Delta X_n \Delta f_n^\top}{\Delta X_n^\top \Delta f_n}\right) G_{n-1} \left(1 - \frac{\Delta X_n \Delta f_n^\top}{\Delta X_n^\top \Delta f_n}\right) + \frac{\Delta X_n \Delta X_n^\top}{\Delta X_n^\top \Delta f_n} \quad (3.8)$$

3.2. Introduction to transition state optimization

Let us define a constraint:

$$\sigma(X) = \sum_{i=1}^m f_i^2(X) = f(X)^\top f(X) \quad (3.9)$$

which meet with searching condition $\sigma(X_e) = 0$. Because of $\sigma(X) \geq 0$, the least square minimization procedure can be applied. Again using Taylor expansion, previous expression can be rewritten as:

$$\begin{aligned} \sigma(X_{k+1}) &= \sigma(X_k) + q_{k+1}^\top V_k + \frac{1}{2} q_{k+1}^\top q_{k+1} + \dots, \\ q_{k+1} &= X_{k+1} - X_k \end{aligned} \quad (3.10)$$

where V_k is a column vector, the elements of which are

$$(V_k)_i = \left(\frac{\partial \sigma(X)}{\partial X_i} \right)_{X=X_k} \quad \text{and} \quad (T_k)_{ij} = \left(\frac{\partial^2 \sigma(X)}{\partial X_i \partial X_j} \right)_{X=X_k} \quad (3.11)$$

If σ attains minimum value then we will obtain $\sigma(X_e) = 0$ and $V(X_e) = 0$. Similar way as in molecular optimization, the nuclei position changes can be derived as:

$$q_{k+1} = -(T_k)^{-1} V_k \quad (3.12)$$

where

$$V_k = 2H_k f_k \quad \text{and} \quad T_k = 2(H_k^T H_k + C_k) \quad (3.13)$$

with

$$(C_k)_{ij} = \sum_{a=1}^m f_a \frac{\partial^2 f_a}{\partial X_i \partial X_j} \quad (3.14)$$

σ can be minimized in similar way in which E itself was minimized, using BFGS procedure already written before.

To make it more practical, let us underline that the molecular optimization is a series of algorithms to get stable structure by seeking minimum energy of observed molecular structure. In case of transition state, the optimization is directed to obtain a transition structure by searching saddle point energy of the observed system (see next illustrative Figure 3.1). Commonly in the molecular reaction, the total energies of observed system at equilibrium (stable structure), both reactant and product are essential for determining enthalpy reaction. While the saddle point energy is important to search the activation energy in such reaction.

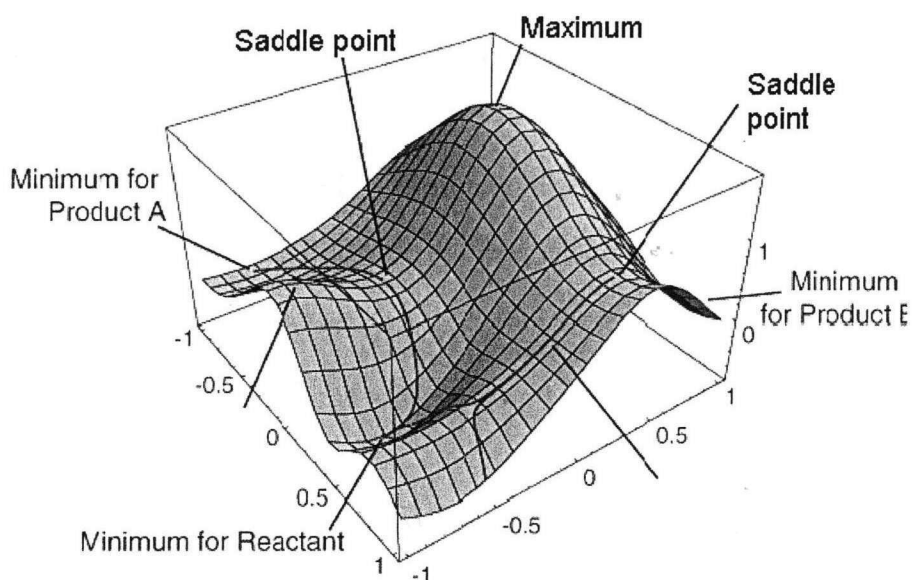
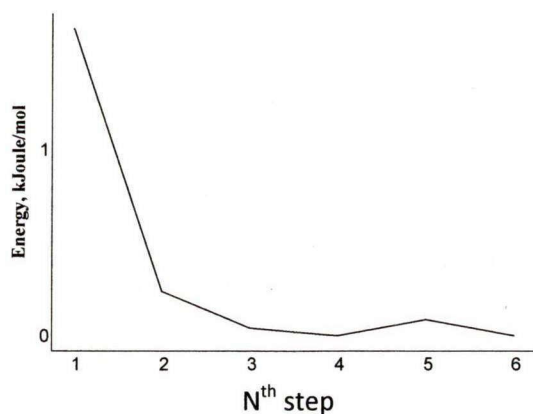


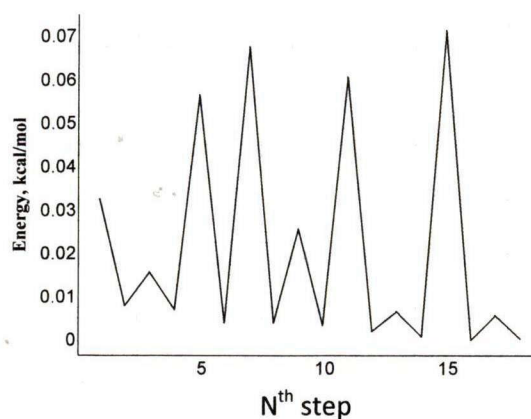
Figure 3.1 An illustration of potential energy surface in a simple reaction, including minimum energy of reactants, product (at equilibriums or stable structure), and an activation energies (at saddle point or transition structure).

Computationally, the success of seeking minima and saddle point energies are determined by the initial structure and the interatomic interaction related to the convergence criterion. For instance, if one chooses bigger convergence criterion such the displacement (ΔX) and the gradient/force (f) at each step of iteration, especially for relative stronger interatomic interaction or in a very close initial structure to equilibrium, it may oscillate the total energy during iteration. Let us review molecular optimization process in simple metal-water cluster for example in $[\text{Ca}(\text{H}_2\text{O})_6]^{2+}$ and $[\text{Fe}(\text{H}_2\text{O})_6]^{2+}$ systems. The Fe-water interaction is relatively stronger than that of Ca-water. We have set for both with similar convergence criterion that are displacement and force. But, in case of Fe-water the initial structure is set to be closer with equilibrium structure, rather than Ca-water one.

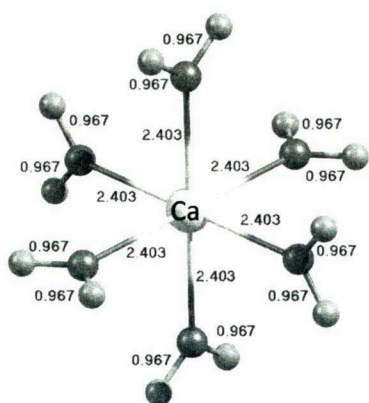
A1



B1



A2



B2

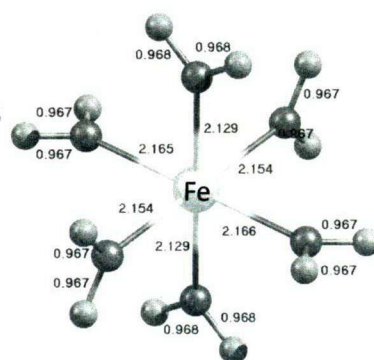


Figure 3.2 (A1) Total energy relative in molecular optimization of $[\text{Ca}(\text{H}_2\text{O})_6]^{2+}$ in each step of converged SCF (self-consistent field), (A2) optimized interatomic distances of $[\text{Ca}(\text{H}_2\text{O})_6]^{2+}$, (B1) total energy relative in molecular optimization of $[\text{Fe}(\text{H}_2\text{O})_6]^{2+}$, and (B2) optimized interatomic distances of $[\text{Fe}(\text{H}_2\text{O})_6]^{2+}$.

As shown in Figure 3.2 (B1), oscillation of total energies is happen during optimization process, in case of Fe-water iteration, and oppositely it is not happen in Ca-water calculation (Figure 3.2 (A1)). For remain figures, Figure 3.2 (A2) and (B2), have shown that M-O distance of Fe-water is shorter than that of Ca-water case indicating its relative stronger interaction.

3.3. A case study on molecular optimization and phase state of small water cluster systems

The optimized structures are essential on approximating the physical phase state of nanocluster of water. The gas phase of water structure can be represented by an optimized structure of isolated water molecule. Intermolecular distances between solid water and liquid water is different. It might be indicated by the intermolecular distances via H—O bond length namely the intermolecular H-bond distance. We have optimized small water cluster with the numbers of molecules are multiple of cage-hexamer (6, 12, and 18) using B3LYP/6-311++G(d,p) level theory.

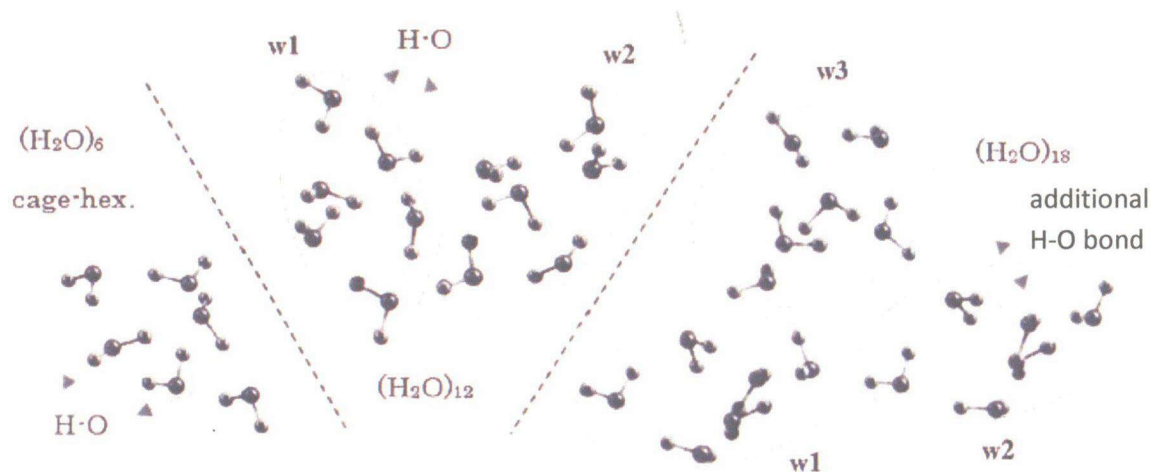


Figure 3.3 Optimized structures of the $(\text{H}_2\text{O})_6$, $(\text{H}_2\text{O})_{12}$, and $(\text{H}_2\text{O})_{18}$ models. The cage like hexamer parts are shown by w1, w2, and w3 and the intermolecular H-bond distances are represented by H—O symbols.

Figure 3.3 shows the optimized clusters of $(\text{H}_2\text{O})_6$, $(\text{H}_2\text{O})_{12}$, and $(\text{H}_2\text{O})_{18}$. Note that there are 3 and 4 additional H-bonds in $(\text{H}_2\text{O})_{12}$ and $(\text{H}_2\text{O})_{18}$, respectively. The H—O distances and monomer dipole moments are used to characterize the liquid water clusters.

Table 3.1 Averages and ranges of H-O distances in the pure water clusters. The experimental value for the bulk is also shown for reference.

Parameter label (unit)	(H ₂ O) ₆ (origin)	(H ₂ O) ₁₂	(H ₂ O) ₁₈	<i>bulk water</i> ^{exp}
Average for w1 (Å)	1.89	1.91	1.90	
Average for w2 (Å)	-	1.89	1.89	
Average for w3 (Å)	-	-	1.88	
Total average (Å)	1.89	1.90	1.89	
Discrepancy (%)	0	0.61	0.07	
Min-max (Å)	1.69-2.10	1.75-2.14	1.66-2.13	1.59-2.27

Although there are additional H-bonds, Table 3.1 shows that the average H–O distances in (H₂O)₁₂ and (H₂O)₁₈ clusters do not change significantly from those of the original (H₂O)₆ cluster. The maximum discrepancy for both extended systems is only about 0.61% ($\pm 0.01\text{\AA}$). It is a very small discrepancy, even for a weak intermolecular interaction, which is much less than half the minimum–maximum (min–max) H–O distances difference in the bulk liquid system (0.34 Å). The H–O distance as an indicator of the liquid phase state has been well defined theoretically [52]. The number of additional H-bonds in the inter hexamer clusters (connecting w1, w2, and w3) increases with the number of inter-hexamer cluster bindings. However, the local H-bond distance ranges min–max H–O distances are in agreement with a results of a previous investigation [53] as shown in Table 3.1. Based on H—O distances, one can predict that our modelled water clusters are close to liquid bulk water.

3.4. A case study on transition state of cage and cyclic water hexamers

The water hexamer ($n=6$) has two interesting points to be considered. First, by monomer dipole moment probing wherein current studies show that the cluster is supposed to be in the liquid phase [54], a transition from gas to solid phase. Second, the most stable formation of hexamer is still under debate since the current studies have found that based from the theoretical binding energies [55] the book/cyclic formation is more stable as compared with the cage formation.

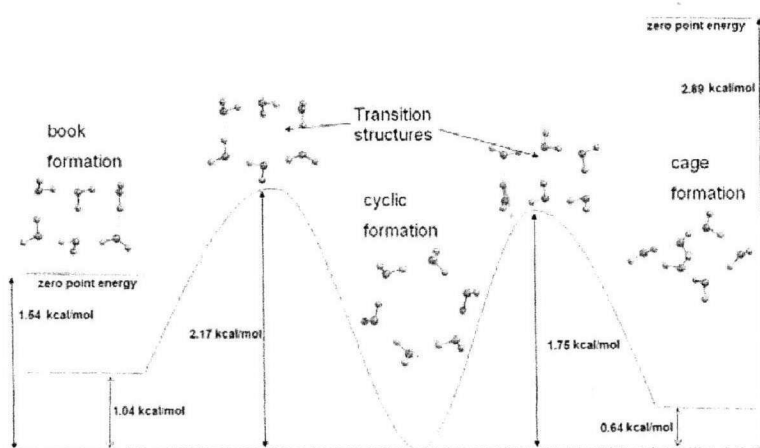


Figure 3.4 The three stable formations of hexamer: cyclic, cage and book formations including their zero point energies, transition formations and the activation energies. The dashed line represents energy reference from cyclic hexamer.

This finding [55] is ambiguous with the fact that very low temperature experimental [56] investigation could probe the cyclic formation beside the previous cage structures finding on hexamer cluster but not for the book formation. Our calculations also show that the cyclic formation is the most stable structure followed by the cage and then the book formation. Zero point energies calculations (cyclic = -287835.44 kcal/mol, book = -287833.90 kcal/mol, and cage = -287832.55 kcal/mol) have changed the order of stabilities as cyclic > book > cage. Nevertheless, after considering the electronic energy, the zero point energies and the activation energies (an energy barrier) through the optimized transitional states as shown in Figure

3.4, we believe that the cyclic formation is more favored and stable than the book and the cage ones. In this case, our calculation results are in agreement with the experimental findings which were also reported that the cyclic hexamer is formed by cyclization process and that rapid quenching inhibits (it supposed to have an energy barrier) its rearrangement to the cage structures [56].

Table 3.2 The number of H-bonding, the average of H-bonding distances and H-bonding strengths from calculated cyclic, book and cage hexamer clusters. Here, H—O distance is the closest distances from H atom in one water molecule to O atom of one another, and H-bond strength is the average binding energy per H-bonding.

Hexamer formation	Number of H-bond	H—O distance (Angstrom)	H-bond strength (kcal/mol)
Cyclic	6	1.74	7.44
Book	7	1.82	6.23
Cage	8	1.92	6.08

The discussion on the water phases with regard to the monomer dipole moment properties is still hard to elucidate the phase of small water cluster system. However, the data from Table 3.2 strongly support that the cyclic hexamer is more rigid than the other hexamers. The cyclic formation has the closest H-bonding distance and the strongest H-bonding energy. As opposite, the cage one has the longest H-bonding distance and the lowest H-bonding energy. Based on the H-bonding distances, H-bonding strength and the monomer dipole moment (MDM) calculations, we predict that the cyclic hexamer has solid phase state and the cage one has liquid phase formation. As a note that phase state order based on H—O distance will follow the reverse order based on monomer dipole moment, those are $\text{H—O}_{\text{solid}} < \text{H—O}_{\text{liquid}} < \text{H—O}_{\text{gas}}$ and $\text{MDM}_{\text{solid}} > \text{MDM}_{\text{liquid}} > \text{MDM}_{\text{gas}}$.

Chapter IV

Small Water Clusters Role in Fuel Cell Membrane

Today, there are two challenges in proton exchange membrane fuel cell (PEMFC) studies. The first is the development of alternative catalysts to platinum [57–62] and the second is solution to the membrane degradation problem [63–67]. Membranes have a principal function of conducting protons from the anode to the cathode. The water content [63–64] of the PEM [65] (electrolyte) has become one of the important subjects of investigation for preventing the membrane function debasement [66]. It is well known that the movement of a proton with alien cationic ions directly affects the water flux and proton conductivity of membranes, causing membrane degradation [67]. Na(I) and Ca(II) ions originally contained in Nafion membranes as contaminants may go into the water and consequently accelerate the degradation [67]. Nevertheless, a comparative study of very low concentration ions has shown that Ca(II) does not only improve the water content or resolve kinetic current degradation problems as compared with the Na(I), but it also has a more competitive mass density [68] (volume contraction effect).

Theoretical investigations on the effects of adding Na(I) and Ca(II) ions to a small water cluster system, especially in order to address its advantages in PEMFC applications, are still rare and therefore desired. Since the electronic structures of both impurities have an s-type orbital, for further orbital analyses, the use of Fe(II) as a comparable cation could be a tractable proposition. In addition, as a flow inside the H-bond channel (Grotthuss mechanism [69–73]), the proton transport is strongly supported by water molecule dynamics through the well-known mechanism [74–76]. Physical insights from molecular bonding perspectives between cations and water are needed to elucidate the water dynamics flexibility in the clearly conflicting requirements inside the cationic system. In this paper, we proposed a theory for the evaluation of the cationic effects of Ca(II), Na(I), or Fe(II) addition to water by proposing definitions of index parameters for the ionization strength, volume expansion, and water rotational rigidity

(at small rotational angles) of cationic aqueous systems by first-principles calculations based on the density functional theory.

4.1. Computational Method

The liquid model of water clusters is optimized using Gaussian version 03 [45] software for the UB3LYP level theory. As a first step, the initial structure of the optimized liquid hexamer $(\text{H}_2\text{O})_6$ is taken from our previous work [73] and the spin configuration is set into singlet state on the neutral charge condition. Second, we have generated the structure of $(\text{H}_2\text{O})_{12}$ and $(\text{H}_2\text{O})_{18}$ by adding one and two more optimized liquid hexamers, respectively into the initial one. The optimized water models have been analyzed by evaluating the H-bond distances and the monomer dipole moments [73]. Theoretical studies using the molecular dynamics method have shown that the coordination numbers of the first water layer are 5.2 [77], 6–7 [78, 79], and 6 [80] for the Na^+ , Ca^{2+} , and Fe^{2+} systems, respectively. In addition, experimental studies have also found that the coordination numbers are in the range of 4–6 [81–83], 6–8 [84–86], and 6 [87] for Na^+ , Ca^{2+} , and Fe^{2+} systems, respectively. On the basis of these values, in this study, the coordination number for the first water layer is assumed to be 6. An octahedral form was chosen as the initial structure of the first water layer, where the negative sides of water (or O atoms) facing the central cation, followed by setting water molecule planes perpendicular to each other. Considering dipole–dipole water attraction directions for the second water layer, we locate water molecules for bonding to each hydrogen atom in the first water layer to design the second layer. Thus, we have 18 water molecules in each ion–water system.

We employ different basis sets for metal cations and water molecules (composed of an O atom and H atoms) since cation atoms have a relatively large number of electrons. The density Gauss double zeta valence plus polarization (DGDZVP) basis set is chosen for the cations (sodium, calcium [45] and iron atoms [88]). However, for atoms in the water molecule, the 6-311++G(d,p) basis sets are used instead. Here, counterpoise energy corrections have been applied to check for basis-set superposition errors

(BSSEs). We also use the natural bond orbital (NBO) [89] population scheme for charge transfer mechanism analysis and atomic charge calculations. The energy barrier per water molecule in the following dehydration reaction is close to their average intermolecular binding energy per water molecule: $\text{Ca}[(\text{H}_2\text{O})_6]^{2+} \rightarrow \text{Ca}^{2+} + 6\text{H}_2\text{O}$. The difference is approximately 2.4% estimated by stretching out water molecules from the central cation. We therefore have approximated the ionization strength of the cationic aqueous systems using the average intermolecular binding energy of the first water layer. We also have expanded the concept for a larger number of water molecules ($n=18$) by assuming a dehydration energy equal to the hydration energy. The second water layer hydration of the cationic aqueous cluster might be written as $\text{Ca}[(\text{H}_2\text{O})_6]^{2+} + 12\text{H}_2\text{O} \leftarrow \text{Ca}[(\text{H}_2\text{O})_{18}]^{2+}$. By using a similar formalism, the average intermolecular binding energy per water molecule, $E_{\text{cat-wat}}$, and the ionization strength of the cationic aqueous system, W_{ion} , are expressed as

$$E_{\text{cat-wat}}^1 = \frac{E[\text{Cation}] + 6(E[\text{H}_2\text{O}] - E[\text{Cation}(\text{H}_2\text{O})_6])}{6}, \quad (4.1)$$

$$E_{\text{cat-wat}}^2 = \frac{E[\text{Cation}(\text{H}_2\text{O})_6] + 12(E[\text{H}_2\text{O}] - E[\text{Cation}(\text{H}_2\text{O})_{18}])}{12} \quad (4.2)$$

and

$$W_{\text{ion}}^k \equiv \frac{E_{\text{cat-wat}}^k}{E_{\text{wat}}^{6(2k-1)}} - 1, \text{ and } k = 1, 2 \quad (4.3)$$

where $E_{\text{cat-wat}}^k$ is the average binding energy of the water molecule in the k -th layer of the cationic aqueous system, $E[\text{Cation}(\text{H}_2\text{O})_n]$ represents the total energy of the cationic aqueous system with n number of water molecules, $E[\text{Cation}]$ is the total energy of the cation, $E[(\text{H}_2\text{O})]$ represents the total energy of a single isolated water molecule, W_{ion}^k is the ionization strength of the k -th water layer of the cationic aqueous system, and $E_{\text{wat}}^{6(2k-1)}$ represents the average intermolecular binding energy of a pure water cluster with $n=6(2k-1)$ molecules. Equations (4.1) and (4.2) correspond to the average H-bond energies needed to decompose an ion–water cluster into water molecules (in the k -th layer) and a cation. Equation (4.3) implicitly describes the relative ionization strength

of a cationic aqueous cluster for a pure water cluster of the same size, of which the average intermolecular binding energy $E_{wat}^{6(2k-1)}$ or E_{wat}^n is given by

$$E_{wat}^n = \frac{n(E[H_2O]) - E[(H_2O)_n]}{n} \quad (4.4)$$

where $E[(H_2O)_n]$ represents the total energy of the water cluster with n number of molecules. Equation (4.4) corresponds to the average H-bond energy needed to decompose a pure water cluster into its isolated molecules. The ionization strength W_{ion}^k implies that the water cluster is favourable while $E_{cat-wat}^k / E_{wat}^{6(2k-1)}$ gives the relative energy gain of hydration. In other words, if the ionization strength is greater than zero ($W_{ion}^k > 0$), the cluster chooses the hydrated cation; otherwise, the cluster chooses the dehydrated one. The temperature effects manifested by thermal and enthalpy energy corrections of the total energy are taken into account by statistical mechanics using the G03 [45] program. Although the thermal energy corrections are calculated from the contributions of translational, vibrational and rotational energies, the enthalpy energy correction is proportional to the gas constant and the temperature of the system.

The volume expansion index formalism is needed to classify the volume variation effects of the hydrated cation. In this case, an implementation of finite temperature analysis near the zero point is also substantial to screen out the cationic expansion effects from any thermal expansions. A Monte Carlo integration method [90] is used to obtain the isosurface volumes of the water cluster $(H_2O)_{18}$ and cationic aqueous systems. By referring to a recent study [91], we define molecular volume as the volume of a contour of 0.001 e/bohr^3 . Then, the electronic isosurface volume expansion index V_x is expressed as

$$V_x = \frac{V_{cat-wat}}{V_{wat}} - 1 \quad (4.5)$$

where $V_{cat-wat}$ and V_{wat} represent the isosurface volumes of the cationic aqueous and octadecamer water clusters, respectively. Equation (4.5) indicates a volume expansion status of a water cluster caused by the addition of one cation. In this case, a fine

integration by about 50 points per cubic Bohr is taken into account. Clearly, the state of $V_x > 0$ implies volume expansion; otherwise, it describes volume contraction.

In addition, we elaborate the parameters from eqs. (4.1), (4.2) and (4.5) into the index X_c for internal pressure estimation induced by cation addition as

$$X_c \equiv \frac{\Delta E}{\Delta V} = 18 \times \frac{E_{cat-wat} - E_{wat}}{V_{cat-wat} - V_{wat}} \quad (4.6)$$

where $E_{cat-wat}$ and E_{wat} represent the average intermolecular binding energy per water molecule of the cationic and pure aqueous systems, respectively. Equation (4.6) basically describes the cation addition effect on the internal pressure, which is responsible for the volume variation. The smaller the X_c , the lesser the volume varies.

The water rotational rigidity of the cationic system is defined by the summation of the total electronic energy and the total nuclear–nuclear repulsion energy obtained by a single-point calculation along the water molecule rotation path (from angle $\theta=0$ to 10°). The water rotational rigidity energy $E_{rot}(\theta)$ at each rotational angle can be expressed as:

$$E_{rot}(\theta) = E_K(\theta) + E_p(\theta) + E_{e-e}(\theta) + E_{N-N}(\theta) - E_{eq} \quad (4.7)$$

where $E_K(\theta)$ represents the non-interacting kinetic energy, $E_p(\theta)$ is the nuclear–electron attraction energy, $E_{e-e}(\theta)$ represents the inter electron Coulomb repulsion and exchange–correlation energy, $E_{N-N}(\theta)$ is the nuclear–nuclear repulsion energy, E_{eq} represents a constant calculated from the minimum total energy at equilibrium, and θ is the rotational angle. The first three terms in eq. (4.7) are obtained by a self-consistent-field (SCF) iterative procedure. In order to identify the contribution of the kinetic energy E_K , the next three terms (excluding E_q) in eq. (4.7) are combined and compared with E_K .

4.2. Physical phase state and molecular binding strength

The contained water is in the liquid phase state to maintain the membrane functionalities, since the degradation is accelerated under dry condition [69] (solid/gas phase state). There are many liquid water models with hydrogen ions in diluting the water structure. The effects of free protons in the pure water system can be neglected by setting the working environment at pH 7 and assuming that the protons will only pass through the membrane [70]. It is difficult to locate the proton at the center of tetrahedral water cluster as a result of weak cation-water dipole attractions. In the case of modelling bulk water in small clusters, the simplest approximation is by taking the generally accepted structures of the small cluster model and then examining the phase state using the electronic dipole and/or the H-bond distance properties. A study of the periodic boundary model of small water clusters (from two to eight molecules) by setting the inter cluster distances to 9 Å showed that the ionization potential and affinity energies of the clusters are close to the values of bulk liquid water [71]. An experimental study showed that cyclic hexamers are in the solid phase state [72]. However, a recent theoretical study by monomer dipole moment calculations showed that the cage hexamers are stable in the liquid phase state [73].

Next, the monomer dipole moments will be evaluated as another indicator. Experimental investigations on the phase states of small water clusters were started in 1996 [93] by focusing on cage hexamer clusters [94] and then on cyclic ones [95]. Recently, studies of 12-water clusters [73] have been performed. It has been found that the cage hexamer is favorable in liquid water [94], while the cyclic one is favorable in the solid phase state [95]. Since a discrepancy is found between the existing theoretical dipole moments of liquid water (~ 3.0 D [96, 97]) and the experimental values (~ 2.45 D [94, 98]), we employ the experimental one as the reference. The monomer dipole moment is approximately proportional to the average intermolecular binding, which is related to both the static and dynamic properties of the matter. We find that more than 50% each of $(\text{H}_2\text{O})_{12}$ and $(\text{H}_2\text{O})_{18}$ is in the liquid state; for simplicity and without loss of generality, we show only a few representatives in Figure 4.1. Thus, the dodecamer and octadecamer clusters are suitable reference for liquid models in order to evaluate the ionization strength of the cationic aqueous systems.

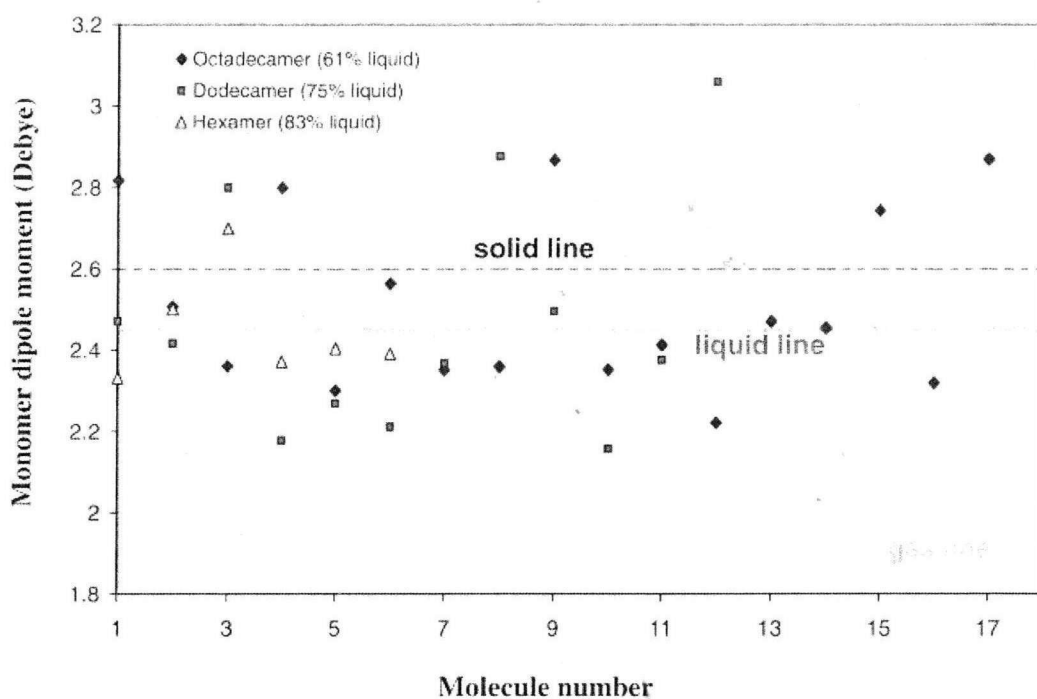


Figure 4.1 Monomer dipole moments of small modeled water clusters [hexamer (H_2O)₆, dodecamer (H_2O)₁₂, and octadecamer (H_2O)₁₈]. Experimental values [80] for the solid, liquid, and gas phases of bulk water are indicated by the corresponding horizontal lines.

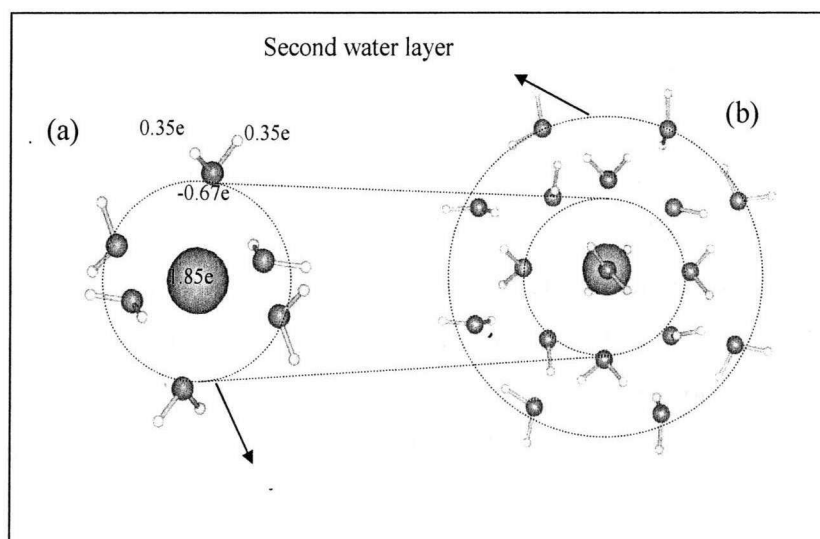


Figure 4.2 The optimized structures of (a) $\text{Ca}[(\text{H}_2\text{O})_6]^{2+}$ (including the cation and water atomic charges) and (b) $\text{Ca}[(\text{H}_2\text{O})_{18}]^{2+}$ formed two water layers. The inner dashed line represents the first water layer and the outer dashed line represents the second water layer in the $\text{Ca}[(\text{H}_2\text{O})_{18}]^{2+}$ cluster.

The total electronic energies and structures of the $\text{Ca}[(\text{H}_2\text{O})_6]^{2+}$ and $\text{Ca}[(\text{H}_2\text{O})_{18}]^{2+}$ systems are optimized to obtain the ionization strengths for each water layer, as shown in Figure 4.2. The atomic charge distributions and water layer structures indicate two types of intermolecular ionization interactions: ion-dipole interactions for the first layer and dipole-dipole interactions induced by the cation for the second layer. Calculated counterpoise energy corrections have shown small BSSEs per number of ion-water bondings within the range of 0.83 – 2.19 KCal/mol, the highest value of which belongs to the ferrous-aqua system.

Table 4.1 Ionization strengths from the first and second layers of Na(I), Ca(II), and Fe(II) aqueous clusters at 0 K and 353.15 K (1.0 atm).

Cation inside	Ionization strength (W_{ion})			
	First layer of water molecules		Second layer of water molecules	
	0 K	353.15 K	0 K	353.15 K
Na(I)	1.70	1.51	0.20	0.20
Ca(II)	5.83	5.22	1.01	0.97
Fe(II)	8.24	7.36	1.09	1.00

We find that the ionization strength of the first water layer is about 5.83 (see Table 4.1), which indicates that the water molecules are strongly bonded to the Ca(II) ion. The average intermolecular binding energy of water clusters increases faster than the cationic aqueous one at a working temperature of 353.15 K. Consequently, the ionization strength decreases to 5.22. The second water layer of the $\text{Ca}[(\text{H}_2\text{O})_{18}]^{2+}$ cluster consists of 12 water molecules or twice of the first one. Its ionization strength is 4.54 less than the first layer. Thus, the binding between the negatively charged water dipoles and the positively charged Ca(II) ion in the first layer is stronger than the dipole-dipole interactions between water molecules in the second layer. Even though, all of the effective intermolecular bindings in the second layer are of the dipole-dipole interaction type, the ionization strength is still twice that of the pure water cluster system. The reduction in ionization strength by 0.04 from the zero point at the working temperature is due to the domination of water dipole-dipole interactions as oppose to the positively charged ion-water dipole interactions in the cationic aqueous cluster of the

second water layer. Now we are ready to compare the Ca(II) aqueous cluster with the Na(I) and Fe(II) ones.

The Ca(II) ion has two positive charges or twice that of the Na(I) one. As a result, the ionization strength of the Ca(II) aqueous cluster for the first water layer binding is higher than that of the Na(I) one. In the case of the Fe(II) aqueous cluster, although the iron cation has the same number of positive charges as the Ca(II) ion, the ionization strength of the iron cation is higher than that of Ca(II) one. The electron spin configuration of the Fe(II) ion is stable in the quintet state, while that of the Ca(II) ion is stable in the singlet state. The larger the number of the unpaired electrons, the stronger the ion spin-dipole attractive interactions between the positively charged cation and the water molecule dipoles. Hence, the ionization interaction strength phenomenon shows up. In the case of the second-water-layer binding, the effects of spin-dipole interactions are screened by the first water layer. Consequently, the ionization strength of the Fe(II) aqueous cluster is almost the same as that of the Ca(II) one. Thus far, the competition between Ca(II) and Fe(II) ions in the electrolyte membrane is still balanced. Thus, we have to examine the ionic volume expansion.

4.3. Volume expansion

The volume variation and the intermolecular/intermolecular binding properties of cationic aqueous systems are key factors in determining the membrane degradation properties. The volume expansion/contraction, the hydration enthalpy energies [74], and the proton mobility [19], strongly depend on those factors. The volume of the water cluster for $n=216$ has accurately been simulated by the molecular dynamics method [76]. Although adding Ca(II) ions to the pure liquid water will occupy some spaces as commonly understood, it is not clear whether the total volume will expand/shrink owing to ion–water interactions. The alternate expansion and contraction of volume can be a serious source for membrane degradation. For instance, the volume variation will produce internal pressures that in turn can cause the breaking of the H-bonds. The best medium for conducting protons through the membrane is pure liquid water [67],

because of its low H-bond strength. However, at a working temperature of 80 C, the low H-bond strength is also responsible for the instability of the conducting channel, inside which protons are propagate. In this case, a higher H-bond strength is demanded.

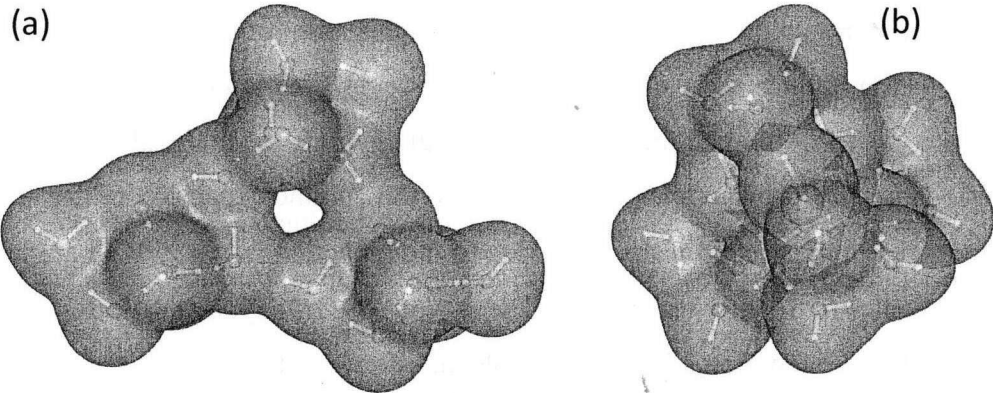


Figure 4.3 Isosurface volumes of the total electronic density at contour 0.001 e.Bohr-3: (a) (H₂O)₁₈ and (b) Ca[(H₂O)₁₈]²⁺ clusters.

The positive and negative signs of the volume expansion index classify the hydration of a solvated cation. The positive hydration characterizes the cationic aqueous system with a negative volume expansion or a shrinking state, and vice versa. Although a cation in an aqueous cluster occupies a small volume at the center of the system, the Ca[(H₂O)₁₈]²⁺ cluster has a positive hydration effect with a 4.76% volume reduction (see Figure 4.3).

Table 4.2 Volume expansion indices V_x , the indices of internal pressure estimation X_c (KCal/cm³) induced by a cation addition, and their qualitative statuses for Na(I), Ca(II), and Fe(II) aqueous clusters.

	Na[(H ₂ O) ₁₈] ⁺	Ca[(H ₂ O) ₁₈] ²⁺	Fe[(H ₂ O) ₁₈] ²⁺
V_x	0.04	-0.03	0.13
X_c	7.05	-45.74	12.50
Status	Swelling	shrinking	swelling

Accordingly, lowering the concentration of the cations by adding water molecules will minimize the shrinking effect on the overall Ca(II) aqueous system. Meanwhile, the swelling state of the Na(I) and Fe(II) aqueous clusters indicates a negative hydration of the systems (see Table 4.2).

In the cases of the Ca(II) and Na(I) aqueous clusters, a high ionization strength implies volume contraction. In other words, the higher the ionization strength, the stronger the cation attracts the water molecules. However, this is not the case for the Fe(II) aqueous cluster. Although the ionization strength is high, the molecular volume is anomalously expanded. The anomaly corresponds to the volume expansion of the villus like substructures in the second water layer due to the reduction in the $\angle\text{HOH}$ angle of the water molecules in the first water layer. The p-type AOs of oxygen are perturbed by the existence of hydrogen atoms in a water molecule, forming the degenerated $1b_2$ (p_x -like), $3a_1$ (p_y -like), and $1b_1$ (p_z -like) MOs. The three MOs play an important role in the bonding and constructions of water molecule. For instance, the $1b_2$ MO forms an antisymmetric pair of OH covalent bonds that repulse each other by increasing the $\angle\text{HOH}$ angle of the water molecule. In contrast, increasing the symmetric $3a_1$ and $1b_1$ MOs by molecular interactions will reduce the $\angle\text{HOH}$ angle. In equilibrium reactions, there are two kinds of orbital charge transfer directions correspond to the cation and water molecule as the targets: forward and backward charge transfers. Some of the backward charge transfers from the cation site to the water molecules site are dominantly received by the $3a_1$ and $1b_1$ -like MOs which reduce the $\angle\text{HOH}$ angle of water molecules in the first water layer. Here, the term of “like” is used for orbitals modified by interactions. The reduction in the $\angle\text{HOH}$ angle will increase the villus like diameter and consequently expand the volume of the cationic aqueous system. This completely explains the anomaly of negative hydration effect on the Fe(II) aqueous cluster.

Again, Table 4.2 shows the pressure indices that clearly signify that the Ca(II) ion has the smallest internal pressure, which is responsible for the smallest volume variation of the corresponding system.

4.4. Water dynamic and proton transport

The rotational rigidity of the water molecule on a cation depicts the proton transport flexibility in the water system. Thus, our next investigation focuses on searching reliable cationic aqueous clusters via water rotational rigidity determination by energetic and electronic analyses. The water rotational rigidity has three main energy contributors, namely, electrostatic, quantum, and steric ones. The quantum contribution consists of the exchange-correlation energy E_{xc} , and the Pauli energy E_p ⁵², which is a portion of kinetic energy that embodies all the effects of the antisymmetric requirement of the total wave function by the Pauli exclusion principle [100]. The steric energy E_s itself represents a Weizsäcker kinetic energy that can be affirmed by atomic, functional group, and geometry [101] contributions. Before we examine the roles of isotropic cation orbitals on reducing the water rotational rigidity, we have to analyze the charge transfer from water to the cation orbital.

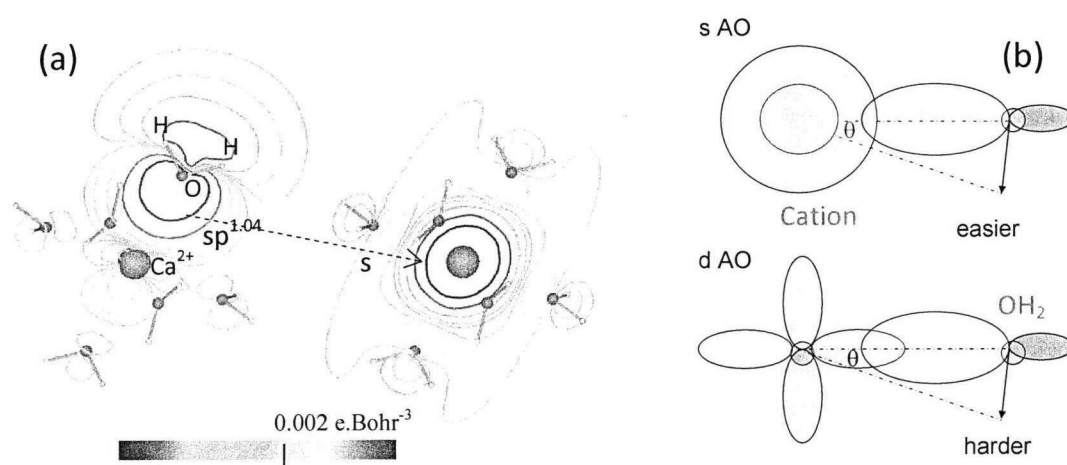


Figure 4.4 (a) Main charge transfer of the $\text{Ca}[(\text{H}_2\text{O})_6]^{2+}$ system from the $\text{sp}^{1.04}$ MO donor at water molecule site to the isotropic AO acceptor at Ca(II) ion site (the outermost contours were plotted at contour $0.002 \text{ e.Bohr}^{-3}$). (b) Schematics of the relation of the rigidity to the ion-water bonding type. Two sketches of molecular bonding between the sp hybrid MOs paired with s -type AO (top site) and d -type AO (bottom site) including their hypothetical barrier results.

In the case of the $\text{Ca}[(\text{H}_2\text{O})_6]^{2+}$ cluster, the electron charges transferred from the $\text{sp}^{1.04}$ hybrid MOs of water molecules are distributed by as much as 81.59, 18.19, and 0.22% relative to those the isotropic s-type AO of the Ca(II) ion [see Figure 4.4(a)], the p-type orbitals of the cation, and the others, respectively. The outermost contour was chosen at 0.002 au in Figure 4.4(a), roughly corresponding to the empirical van der Waals radius [89]. A spherical shape (circular contour) of the s-type orbital at the center of the cluster is formed by the remote-type charge transfer depicting the donor-acceptor MO interactions from the negatively charged water dipole site to the Ca(II) cation site [see Figure 4.4 (b), top]. Meanwhile, in the case of the $\text{Fe}[(\text{H}_2\text{O})_6]^{2+}$ cluster, half of the charge of MO water molecules is transferred to the d-type AO of the Fe^{2+} cation [see Figure 4.4 (b), bottom].

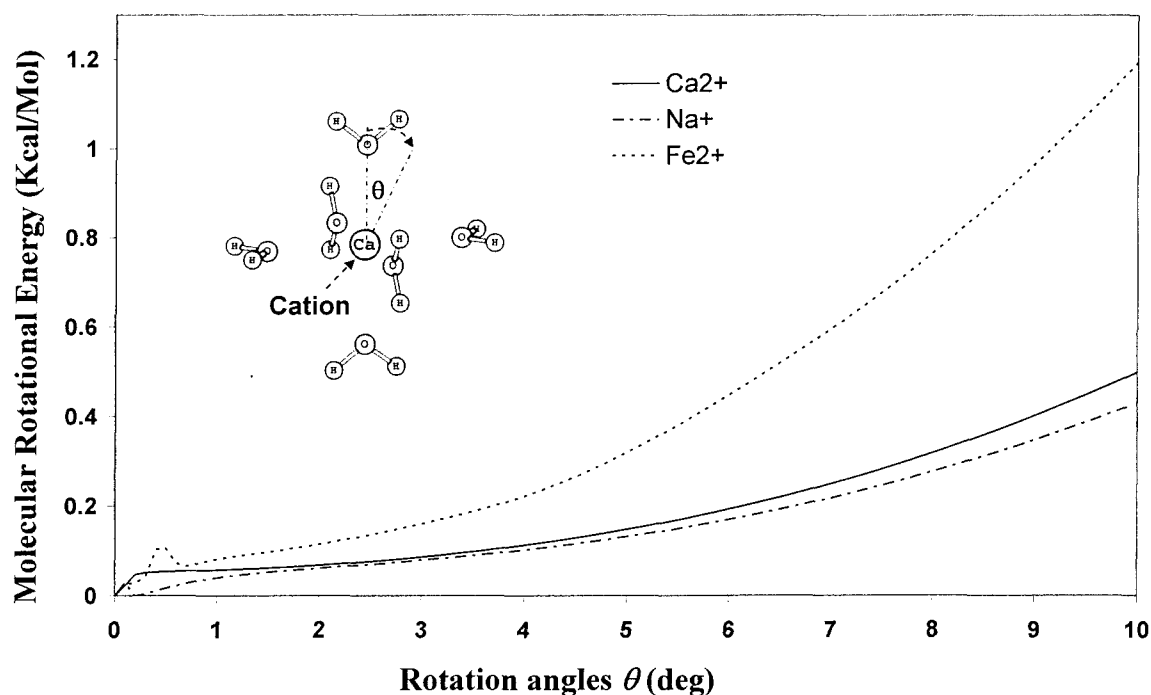


Figure 4.5 Water rotational rigidity energies for $\text{Ca}[(\text{H}_2\text{O})_6]^{2+}$, $\text{Na}[(\text{H}_2\text{O})_6]^{+}$ and $\text{Fe}[(\text{H}_2\text{O})_6]^{2+}$.

For all cationic aqueous systems, the water rotational rigidities resemble a quadratic function in the region of $\theta > 1$ deg (see Figure 4.5). The results indicate that the molecular rotation flexibilities of the $\text{Ca}[(\text{H}_2\text{O})_6]^{2+}$ and $\text{Na}[(\text{H}_2\text{O})_6]^{+}$ systems are

higher than that of $\text{Fe}[(\text{H}_2\text{O})_6]^{2+}$ one. The small peak at $\theta = 0.3$ deg for $\text{Ca}[(\text{H}_2\text{O})_6]^{2+}$ suggests the presence of transitions between spin-dipole bond weakening and strengthening. In the case of the sodium aqueous systems, the charge transfers mostly go to the s-type orbital. Therefore, its water rotational rigidity energies are similar to that of the Ca(II) one.

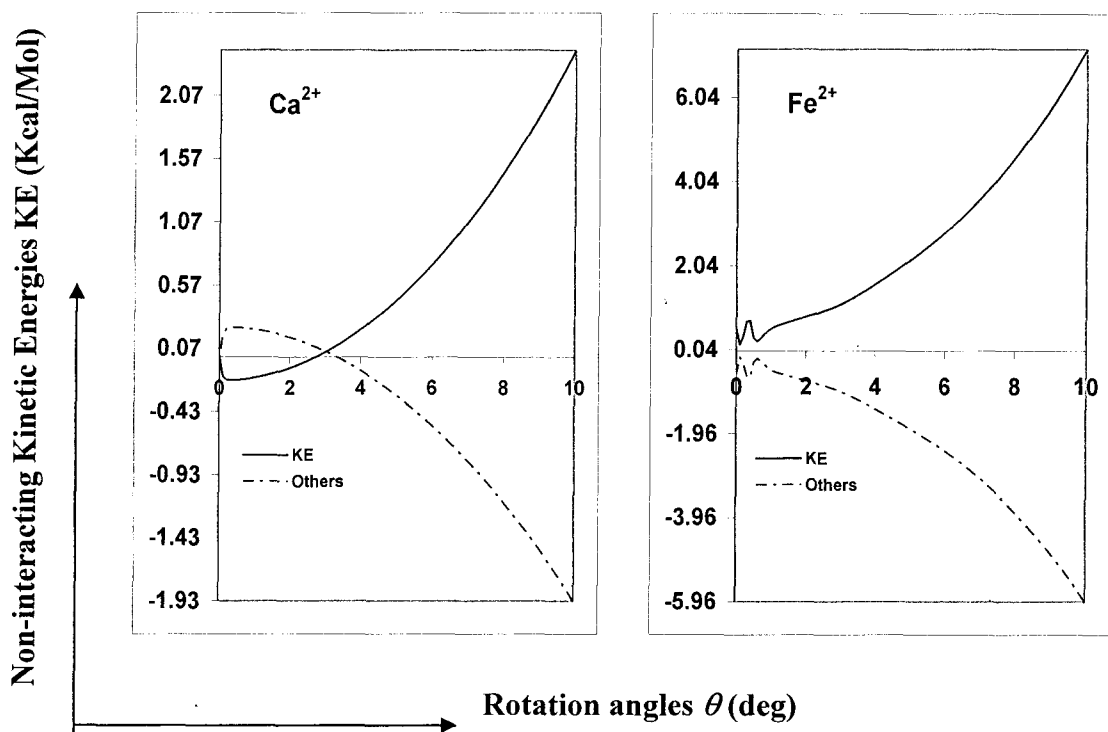


Figure 4.6 Contributions of non-interacting kinetic energies E_K and the others to the rotational rigidity energies as function of the rotational angle for $\text{Ca}[(\text{H}_2\text{O})_6]^{2+}$ and $\text{Fe}[(\text{H}_2\text{O})_6]^{2+}$. We note that the ordinate denotes values measured from the total energy for the equilibrium structure.

Almost all of the formed s-type orbital have spherically symmetric (isotropic) shapes [47] compared with the d-type orbital, which have antisymmetric lobes. This indicates hypothetically that the d-type orbital bondings have higher energy barriers than s-type orbital ones. The difference among energy barriers should be proportional to the Pauli energy plus the steric energy. Figure 4.6 shows a comparison of the non-interacting kinetic energies E_K between the $\text{Ca}[(\text{H}_2\text{O})_6]^{2+}$ and $\text{Fe}[(\text{H}_2\text{O})_6]^{2+}$ clusters,

which represent the Pauli and steric energy contribution. A substantial difference between E_K and the other energy contributors for both cationic aqueous clusters strongly indicates that the proposed energy ($E_p + E_s$) has a large contribution to the total energy barrier. The other energies (non- E_K) represent the remaining energy contributions which close to a quadratic decreasing about 1.92 and 5.67 KCal/Mol (at $\theta = 10$ degrees) for the $\text{Ca}[(\text{H}_2\text{O})_6]^{2+}$ and $\text{Fe}[(\text{H}_2\text{O})_6]^{2+}$ clusters, respectively.

4.5. An evaluation on cationic impurities in the membrane

The results of the H-O distance variation and monomer dipole moment [103] analyses strongly indicate that dodecamer and octadecamer water clusters are mostly in the liquid phase state. The ionization strength of the $\text{Ca}[(\text{H}_2\text{O})_{18}]^{2+}$ cluster for the first-water-layer binding is lower than that of $\text{Fe}[(\text{H}_2\text{O})_{18}]^{2+}$, while that for the second-water-layer binding is higher than that of $\text{Na}[(\text{H}_2\text{O})_{18}]^+$ and almost the same as that of $\text{Fe}[(\text{H}_2\text{O})_{18}]^{2+}$. The Ca(II) ion addition to the liquid $(\text{H}_2\text{O})_{18}$ results in a volume change of 4%, which is very smallest compared to with the those in the case of Na(I) and Fe(II) ion additions. By charge transfer and non-interacting kinetic energy analyses, we demonstrate that the isotropic nature of the Ca(II) and Na(I) orbitals accounts for the flexible rotation of water molecules around the central cation in an aqueous cluster system, whereas the anisotropic nature of Fe(II) orbitals makes the rotation rigid. Accordingly, we predict that Ca(II) will act as a favorable ion impurity in the membrane.

Chapter V

Single Water Dissociation Effects in Ion-exchange Reaction

Some trivalent cations attack at polyelectrolyte membrane will be evaluated using activation energies of single water molecule dissociation processes.

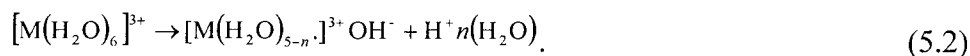
5.1. Related applications

Dehydration has been acknowledged as an essential molecular interaction for water-ion exchange reactions, since some experimental evidences have shown that ion attack at surfactants and polyelectrolyte is followed by its partial interaction with the counter-ions [105-106]. A recent study on counter ion-binding (aqueous Al(III) and Cr(III)) related to the ion attack at electrolyte polyvinyl sulphate (PVS) has brought up that hydration enthalpy from coordinated water release within the primary hydration sphere plays a key role in driving binding to PVS [107]. Similar reactions possibly occur in humid membranes of fuel cells, when contained water is starting dehydrated at working temperature. The residues of dehydrated cations [108] (e.g. Al(III) and Fe(III)) may attack and deactivate the proton hopping supports in the membrane (SO_3^- end). Such interactions can impair the functionality of membranes through protons migration.

It has been stated that hydration enthalpies of $[\text{M}(\text{H}_2\text{O})_6]^{3+}$ clusters, where M denotes the metal ions, influences the amount of reaction product in water and ion exchange reactions. However, contemplating a complete reaction path, the amount and variety of reaction products are not only related with the hydration enthalpy, but also or even more dependent on the activation energy [109] particularly for dehydration reaction. Therefore, it is essential to understand the reaction properties in physiochemical terms such as activation energies and microscopic mechanisms behind them. So far, we have hypothesized that activation energies are affected by the dehydration mechanisms and the central metal properties. However, proof of the hypothesis is still insufficient.

There is a possibility that both amount and variety of products estimated by recent

enthalpy calculation [110] might be different from the products following the minimum reaction path. This likelihood is reasonable, because the hydrated metal ions may have more than one dehydration reaction options. For example, let us consider the following reactions:



The dehydration will produce n pure water molecules by eq. (5.1) and mixed hydroxide and proton by eq. (5.2). For instance, in case of $n=1$, both (5.1) and (5.2) denote dissociative reaction of a single water molecule from $[M(H_2O)_6]^{3+}$ systems or M(III)-water clusters. And possibly there still exist the other reactions as the options. Since the activation energy depends on the dehydration products, a scheme to obtain proper reactions is demanded.

Indeed, the interaction of metal ion with the primary shell of water molecules only involves a central cation and six water molecules. So, if each physical properties of water molecules and the total charges of systems are unchanged in the sequence of M(III)-water clusters then a hypothesis that the favourable reaction path might be controlled by electronic properties of the central cation becomes admissible. This study presents first principle calculations to clarify the validity of the above hypothesis by considering the electronic properties of central cations, (particularly for the first-row transition metal) and analysing mechanisms of single water dissociation from $[M(H_2O)_6]^{3+}$ systems.

5.2. Computational methods

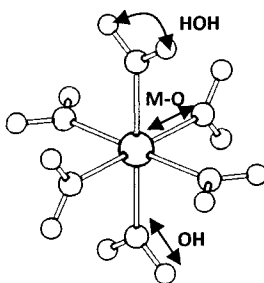


Fig. 5.1 Structure model of $[M(H_2O)_6]^{3+}$ systems as the initial structure for single water molecule dehydration.

As an initial state of the dehydration process, the structures of transition metal ion M(III) surrounded by the first hydration sphere of water molecules (fig. 5.1) were optimized using uB3LYP theory level with separated basis set; the 6-311++G(d,p) for H and O atoms and the DGDZVP [111] for metal ions. Using similar structure models and methods, some possible spin configurations were also optimized to get the ground state energy of the observed systems. In case of dissociative reactions, an optimization technique using synchronous transit-guided quasi-Newton [112] (STQN) method was employed to realize a transition structure by searching a saddle point energy which is guided from both the reactant and the products. Here, the model of products has been obtained by using the minimum potential energy curve (PEC) scan whose procedure will be discussed later. Thus, while stabilization energies (or molecular binding energies) were calculated from the energy difference between reactants and products [113], the activation energies are determined by subtracting the saddle point energy with the initial ground state energy. In addition, vibrational frequency calculations have been performed to assure that only one imaginary frequency can be accepted [114].

A cation-dipole (water) binding interaction can be simply expressed using a classical electrostatic formulation [11]:

$$E_{es}^{i-d}(R, \theta) = -k \frac{Q_1 |\mu_2|}{R^2} \cos(\theta), \quad (5.3)$$

where E_{es}^{i-d} , R , Q_1 , μ_2 , and θ represent the ion-dipole interaction strength, the distance between the ion and the center of the dipole, the ion charge, the monomer dipole moment (MDM), and the angle between the dipole orientation and R direction, respectively. Two indices (1, 2) are assigned to the metal ion and one water molecule, respectively. k is an arbitrary proportional coefficient. A maximum interaction can be obtained by setting θ equal to zero. In eq. (5.3), it is assumed that the change of the other energy contributors such kinetic energies is negligible in the ion-dipole interaction. Another interaction (reaction) energy quantity is given with total energies of reactants and products obtained by first-principles DFT calculations energy as follows [116]:

$$E_{cat-wat} = \frac{E[\text{Cation}] + 6(E[\text{H}_2\text{O}]) - E[\text{Cation}(\text{H}_2\text{O})_6]}{6}. \quad (5.4)$$

Here $E_{cat-wat}$ is the average cation-water binding energy being calculated, $E[\text{Cation}]$ is the total energy of cation, $E[\text{H}_2\text{O}]$ is the total energy of a single isolated water

molecule, and $E[\text{Cation}(\text{H}_2\text{O})_6]$ is the total energy of the cationic water cluster. Although eq. (5.4) does not provide information about local ion-dipole interactions represented by the electrostatic approach in eq. (5.3), but by ignoring inter-neighbour water interactions, we may obtain an average value of binding energies between the water molecules and the metal ion. A more convenient index which is comparable with the experimental hydration enthalpy per water molecule can be written as[117]:

$$\Delta H_h^o = -E_{\text{cat-wat}} + \frac{\Delta E_0 + \Delta E_{\text{sol}} + n\Delta H_{\text{vap}} + \Delta nRT}{n}, \tag{5.5}$$

where ΔE_0 , ΔE_{sol} , n , ΔH_{vap} , R , and T stand for the zero-point energy, solvation energy, the number of water molecules, the vaporization energy, the pressure effect energy, the gas constant, and the temperature, respectively. Using eq. (5.4), one can evaluate original effects of the total electronic energies on the average intermolecular binding at equilibrium and by eq. (5.5) one may compare and validate the analysis method used in experiments. Even though using scaling procedures in some cases, eq. (5.5) had worked well [118,119] however, the second term still needs corrections for better agreements with the experimental data [120].

For better understanding on the interactions of cations with water molecules, more proper analyses of electron population [121-125] and the electronic structure are required.

Table 5.1 Absolute hardness for some monoatomic cations [126].

	η (eV)		
	M	M(II)	M(III)
Cr	3.06	7.23	9.1
Mn	3.72	9.02	8.8
Fe	3.81	7.24	12.08
Co	3.6	8.22	8.9
Ni	3.25	8.50	9.9

In general, a triply charged system has higher absolute hardness than neutral one (see table 5.1) which reduces the correlation effects in the electronic interactions [126]. As the first step, evaluations on charge densities [127] and d-orbital distributions [128]

are necessary. For that purpose, the outermost surfaces of both *d*-orbital lobe and atomic charge density of the triply charged transition metals are plotted as contours at $0.03e/a.u.^3$. Further, since in crystal field potential (CFP) theory had been stated that the formation of (field potential) ligands around a transition metal ion could affect the *d*-orbital splitting (Δ) energy of the central metal ion, and ligand field theory [129] (LFT) resolves this splitting to be equivalence to the t_{2g} - e_g molecular orbitals (MOs) energy gap, so that in this study, the molecular orbital theory based on frontier orbitals (FOs) is taken into consideration as an alternative theory for the electronic interactions elucidation.

The second order of unrestricted Møller–Plesset perturbation [130] (UMP2) method has been employed to produce the orbital energies of M(III)-water clusters. Along with configuration interaction, the perturbation method has been widely used for analysing the total electronic energies [131] and the orbital energies [132,133]. The detail of perturbation method including its analytical derivation had been reviewed elsewhere [134]. A lower order (2nd) perturbation is chosen by considering an investigation result from Leininger, et al [135]. In order to distinguish degenerate MOs from non-degenerate MOs, the density of states (DOS) equivalence has been also taken into account and plotted using Gaussian functions convolution [136] over the orbital energies whose full width at half maximum (FWHM) is set to 0.333.

The dipole moments are derived quantity yielded by electron population analysis. As the bases for evaluating the dipole moments of M(III)-water clusters, the atomic charges underlying natural population analysis (NPA) [123,124] have been employed. In case of PEC scanning for single water dissociation, the dipole moment of Fe(III)-water and Cr(III)-water clusters are computed by adhering each reaction coordinate step. This evaluation would give advantage in observing deprotonation processes during single water dehydration. In addition, the dipole moment changes play an essential role in vibrational frequency visibility in infrared spectroscopy. However, experimentally, it is arduous to produce infrared spectra for molecular systems which has small dipole momenta [138]. In this study, the relative infrared spectra for M-O symmetrical stretching modes have been computed using Gaussian 03 program [139]. For the detailed calculation method, one may refer to a study by B. A. Hess et al [140]. By the

same method and basis set, obtained M-O symmetrical stretching frequencies of each $[M(H_2O)_6]^{3+}$ cluster are plotted in one relative vibrational diagram.

Analysis based on PECs is one of convenient method and analysis for obtaining a chemical reaction path which is comparable with a Monte Carlo study [141], especially for lesser number of constraint variables. The optimized structures of $[M(H_2O)_6]^{3+}$ systems were used as the initial structures of dissociative dehydration. Here, the M-O distances were taken into account with only one constraint variable. By updating the Hessian matrix is updated using Broyden-Fletcher-Goldfarb-Shanno (BFGS) algorithm [142] The internal coordinates have been utilized for the next search direction so that the bond stretching second derivatives are transferable and can be easily parameterized in the Hessian matrix [143] For dissociation processes, the M-O step distance is set to 0.1 Å and the number of steps to 50. The relaxed structure in each step has been optimized under standard criteria of maximum atomic force and maximum displacement; that are 3×10^{-4} and 1.2×10^{-2} respectively in atomic units. The PECs method has been also utilized to evaluate the water rotational rigidities. The rigidity evaluation was made by rotating two water molecules (close each other) around the centred metal ions from the angle of 180° to 122° . Here, we have assumed that $[Cr(H_2O)_5]^{3+}$ and $[Fe(H_2O)_5]^{3+}$ systems would have one water molecule dissociated.

5.3. Hydration enthalpies

The computational results will be discussed in two parts, those are related to hydration enthalpies and associated with the activation energies. Reviewing the molecular binding energy and hydration enthalpy is necessary because it can represent the average molecular bond strength of water molecules to the metal ion at the equilibrium structure which provides a good preliminary point of view for further analyses of water molecule dissociation processes.

Table 5.2 Properties of $[M(H_2O)_6]^{3+}$ systems obtained by the calculations together with experimental hydration enthalpies per molecule as references.

M ions	E_{es}^{i-d} (sc.)	Ecat-wat (kJ/mol)	ΔH_h^o (kJ/mol)		$S, \langle S^2 \rangle$	BSSEs (%)
			calc.	expt.		
Cr	518	528	812	760	3/2, 3.75	6.53
Mn	514	534	824	757	2, 6.00	5.84
Fe	523	524	803	738	5/2, 8.75	5.39
Co	508	561	878	775	3, 6.00	4.65
Ni	264	616	1029	-	1/2, 0.75	4.22
Cu	215	625	916	-	1, 2.00	4.43

The calculated hydration enthalpies per water molecule (ΔH_h^o) as shown in table 5.2 approximately reproduces the experimental data. The expectation of spin contamination $\langle S^2 \rangle$ values [144] and basis set superposition errors (BSSEs) [145] have gained the reliability information of the used method based on the unrestricted B3LYP/6-311++G**. However, in detail, the ΔH_h^o differences among metal ions are still not proportional as compared to experiment data, which may leave some questions that could widen the study scope. Therefore, we focus on the electrons density distribution and single water molecule dissociation from total electronic energy which take about 70.85% part of experimental hydration enthalpies.

Recalling equations (5.1) and (5.2), the dehydration may produce n pure water molecules by eq. (5.1) and mixed hydroxide-proton by eq. (5.2). In case of $n=1$, both (5.1) and (5.2) denote dissociative reaction of a single water molecule from $[M(H_2O)_6]^{3+}$ systems or M(III)-water clusters. Substantively, previous average intermolecular binding in eq. (5.4) comes from chemical eq. (5.1) for $n=6$, nevertheless, as another choice of dehydration reaction, one can use eq. (5.2), and possibly there still exist the other reactions as the options.

Before analysing the intermolecular electronic interactions, some related electronic properties of central metal ions will be discussed first. In general, the soft elements are easier to make correlation than the hard elements. For the same metal,

triply charged metal cations are harder than doubly charged ones, and neutral metals are softer than charged metal cations [126]. Therefore, the charge density surface of central metal is essential especially in higher charged metal cations. Let us consider the cation-water interactions, since the charge density of central cation sterically holds the frontier orbitals of water molecules (at nucleophilic site) to get closer to the central cation, thus the surfaces shape of cation charge density may control the frontier orbitals distributions of water molecules around central cation. The unpaired d-orbital distribution of a metal ion (see the next fig. 5.2) determines the surfaces shape of total charge density of the metal ion which may influence its interaction with the surrounding water molecules.

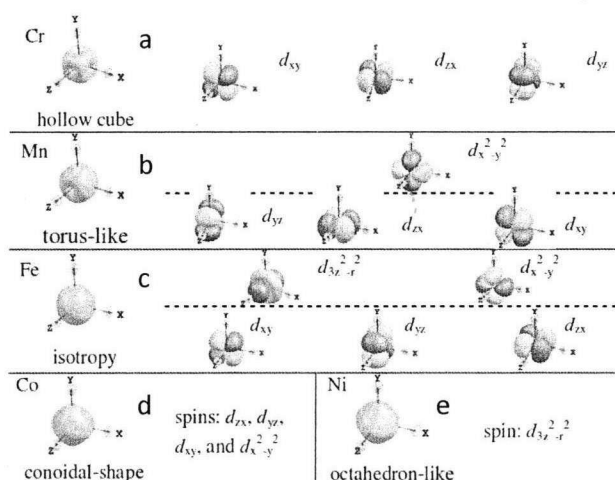


Fig. 5.2 (a) (leftmost) charge density distribution of Cr^{3+} , (right) the unpaired d -orbital distributions of Cr^{3+} ; (b) (leftmost) charge density distribution of Cr^{3+} , (right) the unpaired d -orbital distributions of Cr^{3+} ; (c) (leftmost) charge density distribution of Cr^{3+} , (right) the unpaired d -orbital distributions of Cr^{3+} ; (d) charge density distribution of Cr^{3+} and its spin configuration; (e) charge density distribution of Cr^{3+} and its spin configuration.

For Cr(III) ion, the hollows of the total charge distributions at x , y , z axes are formed by extremely low electron density distribution of the three t_{2g} unpaired electrons at the axes. In case of charge density shape of Mn(III) ion, four hollows at x and y axes are occupied (removed) by an e_g unpaired electron distributions. For the next sequence from Cr(III) to Ni(III) ions, the unpaired electron distributions close the hollows so as to form the cone-shape distributions at x , y , and z axes.

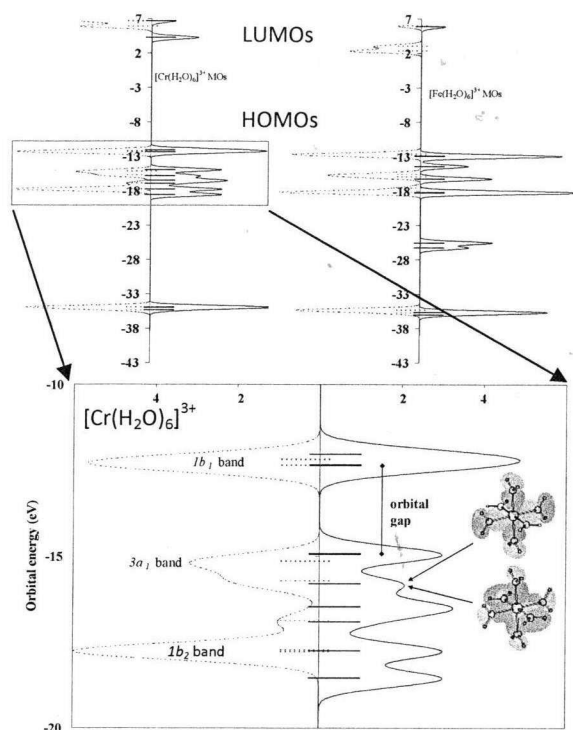


Fig. 5.3 (upper) MOs energy and DOS equivalence for $[\text{Cr}(\text{H}_2\text{O})_6]^{3+}$ and $[\text{Fe}(\text{H}_2\text{O})_6]^{3+}$ systems, (bottom) fine-scale resolution of focused MO energies in $[\text{Cr}(\text{H}_2\text{O})_6]^{3+}$ system, two alpha MOs (inset figure) in group of $3a_1$ band at electron contour 0.03e/a.u.³. The continued lines represent alpha orbital and the dashed ones represent beta orbital.

The influence of molecular orbital (MO) distributions on the structure determination of observed system can be described by frontier orbital theory [146]. The highest occupied – lowest unoccupied MOs (HOMOs-LUMOs) counter-pairs are close together will initiate a charge transfer among MOs to stabilize the formed bond [147]. In case of ion-dipole interactions, beside the bond forming, the induced charges may also result in spatially the shifted electron charge toward the metal ion [148].

The interactions M(III) with $6(\text{H}_2\text{O})$ produce a diverse distribution MOs energies. To facilitate the orbitals analyses, some orbital energies are grouped in a band by keeping up the origin MOs of constituent ligands/water molecules. The MOs energies of $[\text{Cr}(\text{H}_2\text{O})_6]^{3+}$ have been compared with the the MOs of $[\text{Fe}(\text{H}_2\text{O})_6]^{3+}$ to enlighten electronic interaction insight (see fig. 5.3 upper). MOs energies stabilization

in $3a_1$ band at $[\text{Cr}(\text{H}_2\text{O})_6]^{3+}$ has formed MOs orbital gap between $1b_1$ band and $3a_1$ band. The stabilization of MOs has indicated the existence of induced charge from water molecules to Cr(III) ion. As shown in inset fig. 5.3, some MOs have been distributed near the central cation. We strongly argue that this ionic stabilization is caused by electron charge shifting toward the central Cr(III) ion.

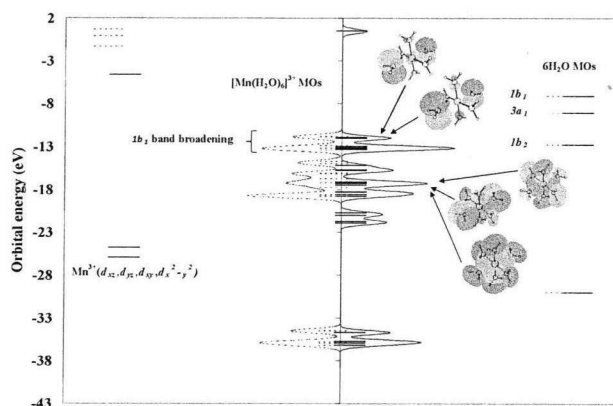


Fig. 5.4 Electronic interactions between Mn^{3+} and $6(\text{H}_2\text{O})$ MOs energies and DOS equivalence of $[\text{Mn}(\text{H}_2\text{O})_6]^{3+}$ system.

In case of the interaction of Mn(III) with $6(\text{H}_2\text{O})$, the broadening of $1b_1$ band in $[\text{Mn}(\text{H}_2\text{O})_6]^{3+}$ system is caused by stabilization-destabilization of MOs energies from d-orbitals of Mn(III) ion and $1b_1$ of H_2O (fig. 5.4). The broadening does not clear in $[\text{Cr}(\text{H}_2\text{O})_6]^{3+}$ and $[\text{Mn}(\text{H}_2\text{O})_6]^{3+}$ system because the d-orbital of both Cr(III) ion and Fe(III) ion have one similar degenerate energy. The destabilized energies are represented by anti-bonding MOs which are responsible for M-O distances elongation and induced charge reduction from water HOMOs. Stabilization of $3a_1$ alpha band closed to $1b_2$ band is caused by inter-water molecules MOs hybridizations.

In addition to electronic properties, a study on molecular structure behaviours and vibrational frequencies will provide us another perspective of M(III)-water interactions. The $3a_1$ and $1b_2$ MOs [149] determine the internal structure of water molecule ($\angle\text{HOH}$ angle and OH covalent bond), while the $1b_1$ MOs determine the external configuration (e.g. an M-O coordination bond and also θ in eq. (5.1)).

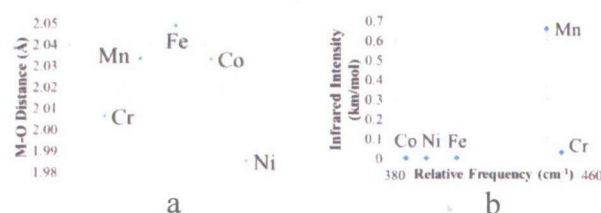


Fig. 5.5 (a) Average M-O distances, and (b) relative vibrational frequencies for symmetrical M-O stretching mode.

Correlating to fig. 5.2, it is seen from fig. 5.5a that reducing number of hollows as increasing the atomic number from Cr(III) to Fe(III) is accompanied by the elongations of M-O distances. They indicate that the some of electron charge of water molecules are induced into the hollows of the Cr(III) charge density. However, in case of Mn(III)-water, Co(III)-water and Ni(III)-water clusters, the distances shorten as increasing the atomic number. This is because the charge density changes to anisotropic so as to form torus-like/cones at the axes and hence to enhance interactions between nearest neighbour water molecules.

An analysis on symmetrical M-O stretching mode (fig. 5.5b) reveals that vibrational frequencies of Cr(III)-water cluster are relatively higher than the others. It has supported our belief that the some electrons induced from water into hollows have made Cr(III) M-O bonds rigid. A higher infrared intensity of Mn(III)-water cluster reflects an anisotropic nature of the M-O distances. In case of Co(III) with single water molecule, experimental study⁴⁶ had exhibited M-O stretching frequency about 410 cm⁻¹.

Table 5.3 Calculated M-O distances of [M(H₂O)₆]³⁺ systems projected onto x, y, and z axes and related experimental data.

Central metal ions	M-O distances (Å)			Expt.
	Calc.			
	x	y	z	
Cr	2	2	2.	1.99 [151,152] (XRD)
	.006	.006	0065	2.01 [153] (EXAFS)
Mn	1.965	1.982	2.153	x= 1.92, y= 1.93, z= 2.13 [154] (EPR)
Fe	2.049	2.049	2.049	1.99-2.05 [155] (XRD, EXAFS, ND), 2.02 [156] (EXAFS)
Co	2.034	2.033	2.032	-
Ni	1.933	1.938	2.084	-

The optimized M-O distances (table 5.3) are in agreement with experimental data, especially for M-O distances of Mn(III)-water cluster. Since the charge density distributions could determine the structures, if so from the optimized structures, one may reversely predict the MOs distributions specifically for the HOMOs. As a reminder, beside the nuclei and electron attractive interaction, the Weizsäcker kinetic energy [157] (which represents a density volume pumping or steric effect [158]) is also related to the electronic shiftings by its charge density gradient.

In case of Cr(III)-water cluster, the $3a_1$ MO of a water molecule has been directly induced into the hollows of the cation charge density. Oppositely, the $1b_1$ and $1b_2$ MOs of the water molecules are repulsively restrained by cationic charge density distribution around hollow edges. Even though the $1b_1$ MOs have minor effects on OH bonds, the $1b_2$ MOs have a substantial contribution to the bonds.

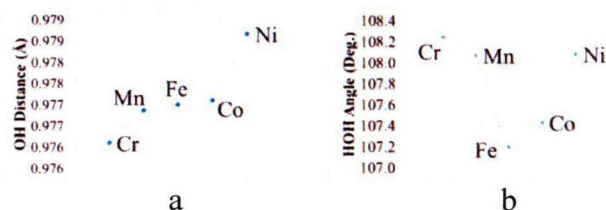


Fig. 5.6 (a) Average optimized OH distances, and (b) \angle HOH angles of $[M(H_2O)_6]^{3+}$ systems.

The OH distances in Cr(III)-water cluster are shorter than the others (fig. 5.6a). They are due to the less volume compression for $1b_1$ and $1b_2$ MOs which conserve the OH distances. Contrary, by increasing the atomic number toward Ni(III), the $1b_1$ and $1b_2$ MOs of a water molecule interact with MOs of the nearest neighbour water molecules and hence elongate the OH distances. The HOH bond angles in Cr(III)-water cluster are wider than the Fe(III) one (fig. 5.6b), since its charge density hollows have made room for the induced $3a_1$ MOs of an approaching water molecule. Just in case of the Mn(III) and Ni(III)-water clusters, the interactions between nearest neighbour water molecules are accountable for the \angle HOH widening

5.4. Single dehydration mechanism and reaction products

Preceding optimized structures of $[M(H_2O)_6]^{3+}$ systems are used as the initial structures for dissociative dehydration scanning.

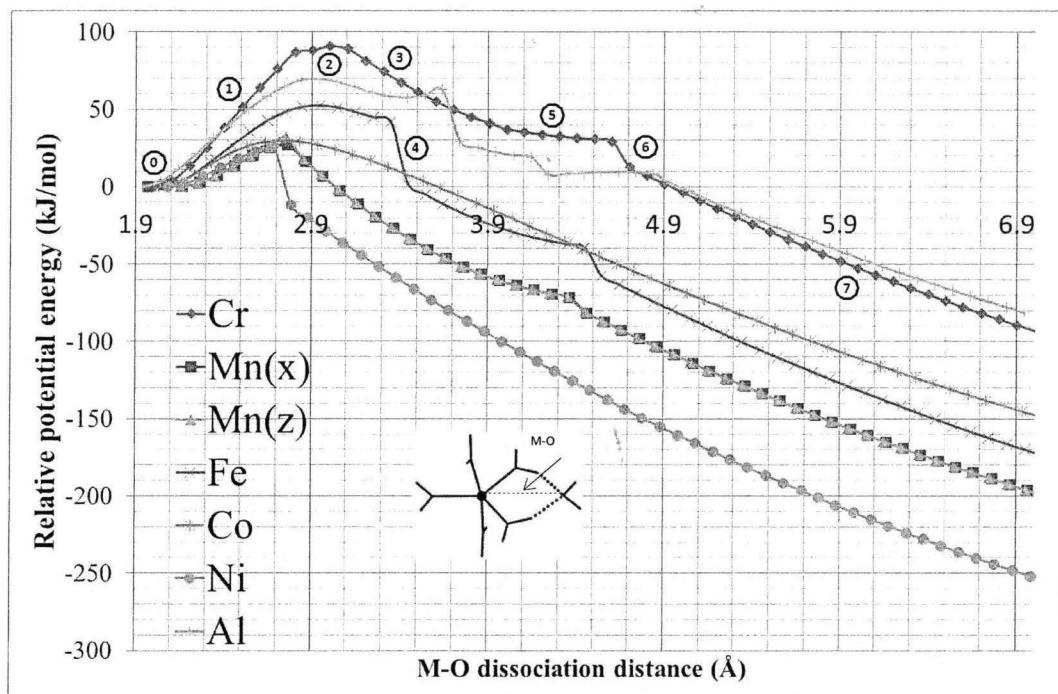


Fig. 5.7 Relative potential energy curves (fully relaxed structure) of $[M(H_2O)_6]^{3+}$ systems ($M=Cr, Mn, Fe, Co, Ni, \text{ and } Al$) which M-O distances are used as constraint variables. The dehydration steps are symbolized by circled numbers. The symbols of Mn(x) and Mn(z) in figure legend stand for single dehydrations for Mn(III)-water cluster at x and z axes directions, respectively.

We have obtained a surprising result that all but the Co(III)-water cluster had shown single dehydration reactions by following eq. (5.2) while only the Co(III)-water cluster has followed eq. (5.1). This means that we have to go beyond the assumption which had used eq. (5.1) as a basis for the hydration enthalpy calculation. The uppermost curve fig. 5.7 is a relative potential energy curve of Cr(III)-water cluster for dehydration reaction of single water molecule. The highest peak of this curve at step of ② represents the activation energy for the dehydration about lesser than 100 kJ/mol, followed by Al(III), Fe(III), Co(III), Mn(III), and Ni(III). The activation energies for Mn(III)-water and Co(III)-water clusters are almost equal. The activation energies of

dehydration for both directions in Mn(III)-water cluster are extremely equal. However, both values are underestimated as predicted from the vibrational frequencies (fig. 5.5b). It is due to the repulsive interaction between $1b_1$ MOs of a water molecule and d -orbital of Mn(III), and also with $3a_1$ MOs of neighbour water molecules at region ①. It then reduces the activation energy.

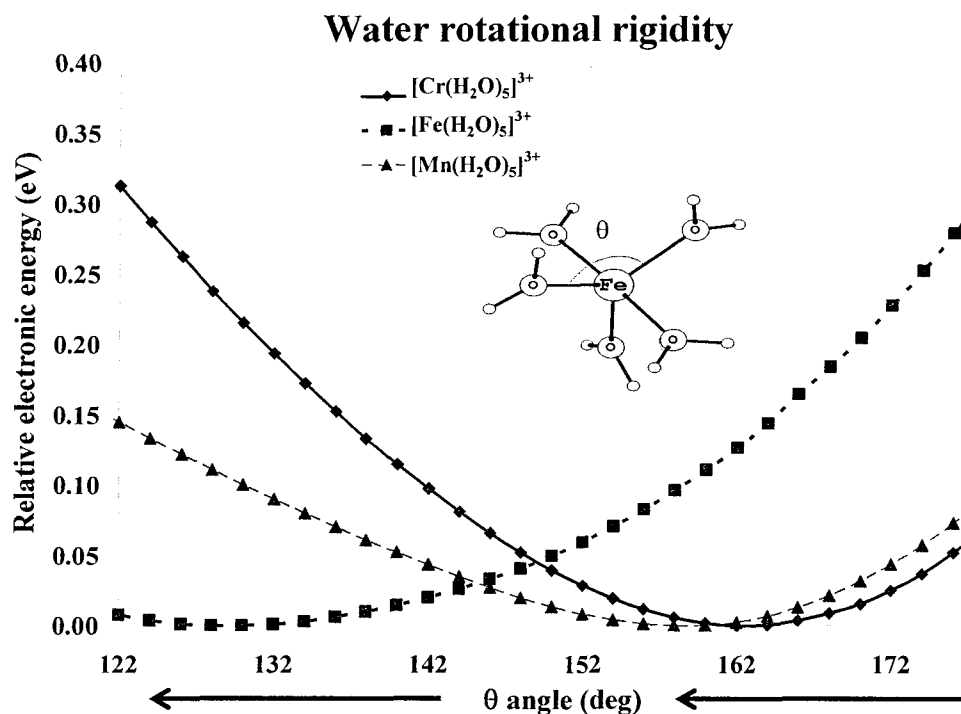


Fig. 5.8 The three PEC calculations of $[\text{Cr}(\text{H}_2\text{O})_5]^{3+}$, $[\text{Mn}(\text{H}_2\text{O})_5]^{3+}$, dan $[\text{Fe}(\text{H}_2\text{O})_5]^{3+}$ systems on water rotational rigidities. The arrows represent a scanning angle direction. Inset figure shows a model example.

Oppositely, for the Fe(III)-water cluster, the activation is overestimated from the vibrational frequencies (fig. 5.5b). Their isotropic charge density of central cation has decreased the water rotational rigidity [117] which has relaxed two neighbour water molecules to gain two H-bonds forming (inset fig. 5.8). The formed H-bond coordinations have conserved the monomer dipole moment and angle θ of the constraint water molecule (eq. (5.3)). The lowest water rotational rigidity by $[\text{Fe}(\text{H}_2\text{O})_5]^{3+}$ system, as depicted fig. 5.8, has proved its contribution on lowering the activation energy. As a note, the angle θ in fig. 5.8 is different from as in eq. (5.3). Except for Co(III)-water

cluster, the steps of ③, ④, ⑤, ⑥, and ⑦ represent two-coordination bond elongation, one-coordination bond breaking, transferring proton to the constraint water, hydronium forming (H_3O^+), and hydronium releasing, respectively. Some clusters have incomplete single water molecule dehydration steps.

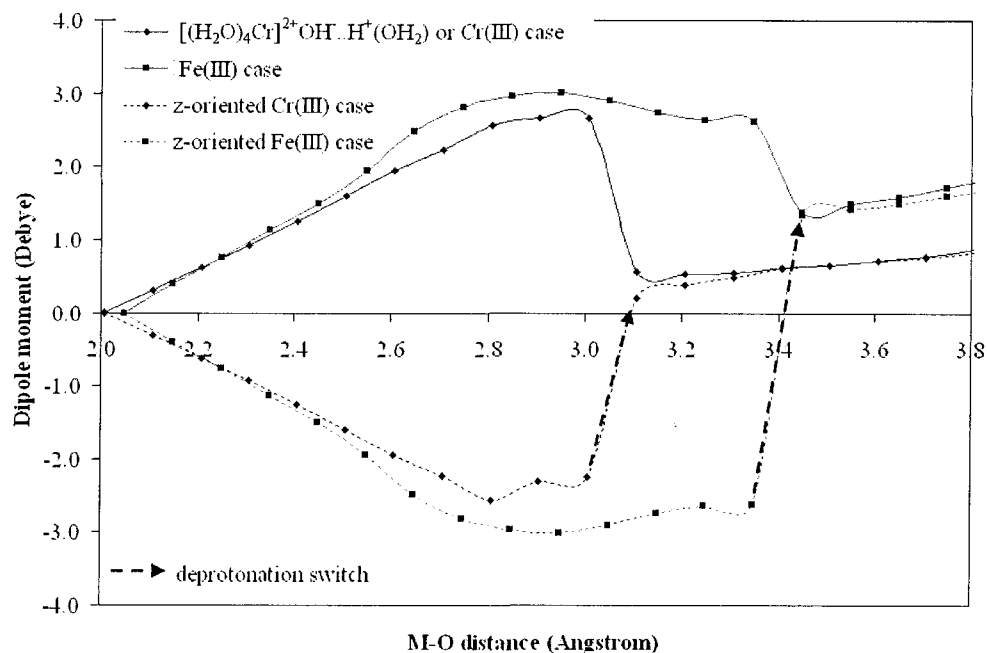


Fig. 5.9 Total dipole moments scanning for $[\text{Fe}(\text{H}_2\text{O})_6]^{3+}$ and $[\text{Cr}(\text{H}_2\text{O})_6]^{3+}$ systems. The dashed lines represent the z-oriented total dipole moments.

It not only indicates that the higher dipole moments scan of $[\text{Fe}(\text{H}_2\text{O})_6]^{3+}$ system has exhibited the occurrence of water rotations (bending) in z-orientation, but fig. 5.9 also demonstrates that the dipole moment switch (dashed arrows) has proved the deprotonation happenings. When a proton (H^+) has left its water molecule (the H_2O has changed to OH^-), the charge being moved has changed the total dipole moment of $[\text{M}(\text{H}_2\text{O})_6]^{3+}$ system. It is a good news for scientist especially experimentalist since infrared spectrometer is relatively sensitive to the dipole moment changes.

In case of Co(III) -water cluster, the dehydration reaction produces a pure water molecule, since the water molecules are isolated from each other.

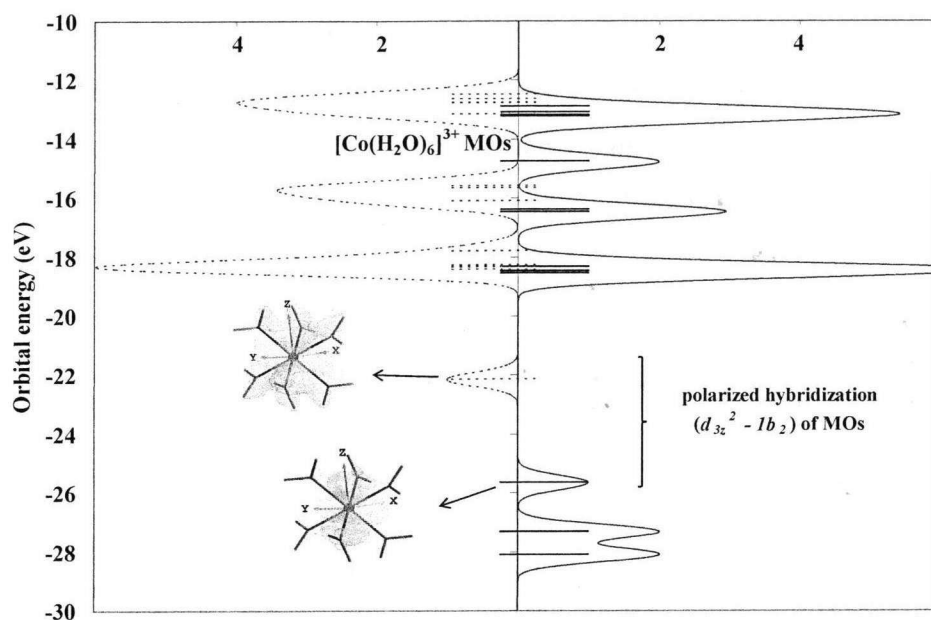


Fig. 5.10 The MOs energy and DOS equivalence of $[\text{Co}(\text{H}_2\text{O})_6]^{3+}$ system. The continued and dashed lines represent alpha and beta orbitals, respectively. Inset figure provides polar hybridized MOs at electron contour 0.03e/a.u.³.

A polarized hybrid MO ($d_{3z^2} - 1b_2$ MO) has been formed as the result of orbitalic interactions between 6 H_2O and central Co(III) ion (see fig. 5.10). In this case, the alpha orbital has been stabilized by a more localized electron distribution to central Co(III), and vice versa for beta orbital. The hybrid MOs have isolated the interaction among water molecules. As a note, the d-orbital filling in Co(III)-water cluster follows high spin configuration, whereas Ni(III)-water cluster obeys low spin filling. It is understandable in FO interactions since the highest cationic orbital energy of Ni(III) ion is lower than that of Co(III). Thus, an higher d -orbital splitting of Ni(III)-water cluster has led to low spin filling.

We believe that the activation energies of the dehydration reactions should be relevant to water and ion exchange reactions, particularly for exemplified metal ion attack at polyelectrolyte. To convince our computational results, the single dehydration of Al(III)-water cluster has been evaluated to obtain comparable stabilities with the Cr(III) and Fe(III)-water clusters. Based on the activation energies (fig. 5.7), we have found that Cr(III)-water cluster is more stable than Al(III)-water cluster. These results do not only explain the higher number of Al(III) binding to PVS than Cr(III) [107], but

they also provide another reasonable explanation for higher membrane degradation level by Fe(III) than that of Al(III) [108] metal ion. Another experimental study [147] on the ion exchange reaction of Al(III) with Fe(III) also supports our results.

Chapter VI

Conclusion

6.1. Summary

Some important results that we can underline in these studies:

1. By preparing reasonable initial structures using both reactivity index from Fukui functions and the symmetry considerations, we could find a more efficient way in obtaining the most stable formations of small water cluster systems. The average binding energies trend for $n = 1-12$ tend to asymptotically converged at the average intermolecular binding value of bulk water.
2. The results of the H-O distance variation and monomer dipole moment analyses strongly indicate that dodecamer and octadecamer water clusters are mostly in the liquid-like phase state. The ionization strength of the $\text{Ca}[(\text{H}_2\text{O})_{18}]^{2+}$ cluster for the first-water-layer binding is lower than that of $\text{Fe}[(\text{H}_2\text{O})_{18}]^{2+}$, while that for the second-water-layer binding is higher than that of $\text{Na}[(\text{H}_2\text{O})_{18}]^+$ and almost the same as that of $\text{Fe}[(\text{H}_2\text{O})_{18}]^{2+}$. The Ca(II) ion addition to the liquid $(\text{H}_2\text{O})_{18}$ results in a volume change of 4%, which is very smallest compared to with the those in the case of Na(I) and Fe(II) ion additions. By charge transfer and non-interacting kinetic energy analyses, we demonstrate that the isotropic nature of the Ca(II) and Na(I) orbitals accounts for the flexible rotation of water molecules around the central cation in an aqueous cluster system, whereas the anisotropic nature of Fe(II) orbitals makes the rotation rigid. Accordingly, we predict that Ca(II) will act as a favorable ion impurity in the membrane.
3. We believe that the activation energies of the dehydration reactions should be relevant to water and ion exchange reactions, particularly for exemplified metal ion attack at polyelectrolyte. To convince our computational results, the single

dehydration of Al(III) cluster has been evaluated to obtain comparable stabilities with the Cr(III) and Fe(III) clusters. Based on the activation energies, we have found that Cr(III) cluster is more stable than Al(III) cluster. These results do not only explain the higher number of Al(III) binding to PVS than Cr(III), but they also provide another reasonable explanation for higher membrane degradation level by Fe(III) than that of Al(III) metal ion.

6.2. Suggestion

For more molecular modelling in the future, it is nice:

1. To study water clustering effect on deprotonation of hydronium,
2. To use molecular dynamic model which is more applicable,
3. To interact the small water with a specific metal surface.

References

- [1] J. Lin, P. H. Wu, R. Wycisk, P. N. Pintauro, and Z. Shi, *Macromolecules* **41** (2008) 4284.
- [2] J. Ozaki, T. Anahara, N. Kimura, and A. Oya, *Carbon* **44** (2006) 3358.
- [3] J. Ozaki, T. Anahara, N. Kimura, and A. Oya, *Carbon* **45** (2007) 1847.
- [4] P. H. Matter, E. Wang, M. Arias, E. J. Biddinger, and U. S. Ozkan, *J. Mol. Catal. A* **264** (2007) 73.
- [5] T. Ikeda, M. Boero, S.-F. Huang, K. Terakura, M. Oshima, and J. Ozaki, *J. Phys. Chem. C* **112** (2008) 14706.
- [6] H. K. Dipojono, A. G. Saputro, R. Belkada, H. Nakanishi, H. Kasai, M. David, and E. S. Dy, *J. Phys. Soc. Jpn.* **78** (2009) 094710.
- [7] M. K. Agusta, M. David, H. Nakanishi, and H. Kasai, *Surf. Sci.* **604** (2010) 245.
- [8] T. Okada, G. Xie, and Y. Tanabe, *J. Electroanal. Chem.* **413** (1996) 49.
- [9] J. St-Pierre, D. P. Wilkinson, S. Knights, and M. Bos, *J. New Mater. Electrochem. Syst.* **3** (2000) 99.
- [10] A. Collier, H. Wang, X. Z. Yuan, J. Zhang, and D. P. Wilkinson, *Int. J. Hydrogen Energy* **31** (2006) 1838.
- [11] F. A. de Bruijn, V. A. T. Dam, and G. J. M. Janssen, *Fuel Cell* **8** (2008) 3.
- [12] X. Cheng, Z. Shi, N. Glass, L. Zhang, J. Zhang, D. Song, Z. S. Liu, H. Wang, and J. Shen, *J. Power Source* **165** (2007) 739.
- [13] T. Okada, Y. Ayato, H. Satou, M. Yuasa, and I. Sekine, *J. Phys. Chem. B* **105** (2001) 6980.
- [14] C. G. Sinn, R. Dimova, and M. Antonietti, *Macromolecules*, **37** (2004) 3444.

- [15] T. Ohki, M. Harada, and T. Okada, *J. Phys. Chem. B*, **112** (2008) 11863.
- [16] H. D. Burrows, D. Costa, M. L. Ramos, M. G. Miguel, M. H. Teixeira, A. A. C. C. Pais, A. J. M. Valente, M. Bastos, and G. Bai, *Phys. Chem. Chem. Phys.*, **14** (2012) 7950.
- [17] H. Li, K. Tsay, H. Wang, J. Shen, S. Wu, J. Zhang, N. Jia, S. Wessel, R. Abouatallah, N. Joos, and J. Schrooten, *J. Power Sources*, **195** (2010) 8089.
- [18] S. Tomoda and K. Kimura, *Chem. Phys. Lett.* **102** (1983) 560.
- [19] S. H. S. Salk, C.K. Lutrus, T.S. Chen, D.E. Hagen, and T. Oshiro, *Tetrahedron* **44** (1988) 7373.
- [20] T. R. Dyke and J. S. Muentner, *J. Chem. Phys.* **59** (1973) 3125.
- [21] G. H. Haggis, J. B. Hasted, and T. J. Buchanan, *J. Chem. Phys.* **20** (1952) 1452.
- [22] C. A. Coulson and D. Eisenberg, *Proc. R. Soc. London Ser. A* **291** (1966) 445.
- [23] R. G. Parr, and W. Yang, *Density Functional Theory of Atoms and Molecule*, Oxford University Press, 1989.
- [24] R. S. Mulliken, *J. Chem. Phys.* **23** (1955) 1833.
- [25] A. E. Reed, R. B. Weinstock, and F. Weinhold, *J. Chem. Phys.* **83** (1985) 735.
- [26] K. Liu, M. G. Brown, and R. J. Saykally, *J. Phys. Chem. A* **101** (1997) 8995.
- [27] T. R. Dyke and J. S. Muentner, *J. Chem. Phys.* **59** (1973) 3125.
- [28] G. H. Haggis, J. B. Hasted, and T. J. Buchanan, *J. Chem. Phys.* **20** (1952) 1452.
- [29] C. A. Coulson and D. Eisenberg, *Proc. R. Soc. London Ser. A* **291** (1966) 445.
- [30] J. Lin, et al., *Macromolecules* **41** (2008) 4284.
- [31] M. Tsuda, Nelson B. A. Jr., and H. Kasai, *Chem. Phys.* **324** (2006) 393.

- [32] Z. Lu, G. Polizos, D. D. Macdonald, and E. Manias, *J. Electrochem. Soc.* **155** (2008) B163.
- [33] S. Tomoda and K. Kimura, *Chem. Phys. Lett.* **102** (1983) 560.
- [34] S. H. S. Salk, et al., *Tetrahedron* **44** (1988) 7373.
- [35] T. R. Dyke and J. S. Muentner, *J. Chem. Phys.* **59** (1973) 3125.
- [36] G. H. Haggis, J. B. Hasted, and T. J. Buchanan, *J. Chem. Phys.* **20** (1952) 1452.
- [37] C. A. Coulson and D. Eisenberg, *Proc. R. Soc. London Ser. A* **291** (1966) 445.
- [38] A. D. Becke, *J. Chem. Phys.* **98** (1993) 5648.
- [39] K. B. Wiberg, *J. Comput. Chem.* **25** (2004) 1342.
- [40] P. Fuentealba, et al., *J. Chem. Phys.* **113** (2000) 2544.
- [41] A. E. Reed, et al., *Chem. Rev.* **88** (1988) 899.
- [42] D. Feller, *J. Chem. Phys.* **96** (1992) 6104.
- [43] S. Kawahara, et al., *Chem. Phys.* **273** (2001) 207.
- [44] L. A. Curtis, D. J. Frurip, and M. Blander, *J. Chem. Phys.* **71** (1979) 2703.
- [45] M. J. Frisch, G. W. Trucks, H. B. Schlegel, G. E. Scuseria, M. A. Robb, J. R. Cheeseman, J. A. Montgomery, Jr., T. Vreven, K. N. Kudin, J. C. Burant, J. M. Millam, S. S. Iyengar, J. Tomasi, V. Barone, B. Mennucci, M. Cossi, G. Scalmani, N. Rega, G. A. Petersson, H. Nakatsuji, M. Hada, M. Ehara, K. Toyota, R. Fukuda, J. Hasegawa, M. Ishida, T. Nakajima, Y. Honda, O. Kitao, H. Nakai, M. Klene, X. Li, J. E. Knox, H. P. Hratchian, J. B. Cross, V. Bakken, C. Adamo, J. Jaramillo, R. Gomperts, R. E. Stratmann, O. Yazyev, A. J. Austin, R. Cammi, C. Pomelli, J. W. Ochterski, P. Y. Ayala, K. Morokuma, G. A. Voth, P. Salvador, J. J. Dannenberg, V. G. Zakrzewski, S. Dapprich, A. D. Daniels, M. C. Strain, O. Farkas, D. K. Malick, A. D. Rabuck, K. Raghavachari, J. B. Foresman, J. V. Ortiz, Q. Cui, A. G. Baboul, S. Clifford, J. Cioslowski, B. B. Stefanov, G. Liu,

- A. Liashenko, P. Piskorz, I. Komaromi, R. L. Martin, D. J. Fox, T. Keith, M. A. Al-Laham, C. Y. Peng, A. Nanayakkara, M. Challacombe, P. M. W. Gill, B. Johnson, W. Chen, M. W. Wong, C. Gonzalez, and J. A. Pople, http://www.gaussian.com/g_tech/g_ur/refs.htm#G03, Gaussian Inc., Wallingford CT, (2004).
- [46] J. Cioslowski, J. Am. Chem. Soc. **111** (1989) 8333.
- [47] M. E. Fajardo and S. Tam, J. Chem. Phys. **115** (2001) 6807.
- [48] H. M. Lee, et al., J. Chem. Phys. **112** (2000) 9759.
- [49] K. Nauta and R. E. Miller, Science **287** (2000) 293.
- [50] A. Szabo, and N. S. Ostlund, Modern Quantum Chemistry, Dover Publication, 1996.
- [51] J. D. Head, and M. C. Zerner, Chem. Phys. Lett. **122** (1985) 264.
- [52] N. Metropolis and S. Ulam, J. Am. Stat. Assoc. **44** (1949) 335.
- [53] R. Kumar, J. R. Schmidt, and J. L. Skinner, J. Chem. Phys. **126** (2007) 204107.
- [54] K. Liu, M. G. Brown, and R. J. Saykally, J. Phys. Chem. A **101** (1997) 8995.
- [55] J. T. Su, et al., J. Phys. Chem. A **108** (2004) 10518.
- [56] K. Nauta and R. E. Miller, Science **287** (2000) 293.
- [57] J. Ozaki, T. Anahara, N. Kimura, and A. Oya, Carbon **44** (2006) 3358.
- [58] J. Ozaki, T. Anahara, N. Kimura, and A. Oya, Carbon **45** (2007) 1847.
- [59] P. H. Matter, E. Wang, M. Arias, E. J. Bidinger, and U. S. Ozkan, J. Mol. Catal. A, Chem. **264** (2006) 73.
- [60] T. Ikeda, M. Boero, S-F. Huang, K. Terakura, M. Oshima, and J. Ozaki, J. Phys. Chem. C **112** (2008) 14706.

- [61] H. K. Dipojono, A. G. Saputro, R. Belkada, H. Nakanishi, H. Kasai, M. David, and E. S. Dy, *J. Phys. Soc. Jap.* **78** (2009) 094710.
- [62] M. K. Agusta, M. David, H. Nakanishi, and H. Kasai, *Surf. Sci.* **604** (2010) 245.
- [63] T. Okada, G. Xie, and Y. Tanabe, *J. Electroanal. Chem.* **413** (1996) 49.
- [64] J. St-Piere, D. P. Wilkinson, S. Knights, and M. Bos, *J. New. Matter Electrochem. Syst.* **3** (2000) 99.
- [65] A. Collier, H. Wang, X.Z. Yuan, J. Zhang, and D.P. Wilkinson, *Int. J. Hydrogen Energy* **31** (2006) 1838.
- [66] F. A. de Bruijn, V.A.T. Dam, and G.J.M. Janssen, *Fuel Cell* **08** (2008) 3.
- [67] X. Cheng, Z. Shi, N. Glass, L. Zhang, J. Zhang, D. Song, Z.S. Liu, H. Wang, and J. Shen, *J. Power Source* **165** (2007) 739.
- [68] T. Okada, Y. Ayato, H. Satou, M. Yuasa, and I. Sekine, *J. Phys. Chem. B* **105** (2001) 6980.
- [69] N. Agmon, *Chem. Phys. Lett.* **244** (1995) 456.
- [70] D. Marx, M. E. Tuckerman, J. Hutter, and M. Parrinello, *Nature* **397** (1999) 601.
- [71] R. Pomés, and B. Roux, *J. Phys. Chem.* **100** (1996) 2519.
- [72] M. E. Tuckerman, D. Marx, and M. Parrinello, *Nature* **417** (2002) 925.
- [73] M. Boero, T. Ikeshoji, and K. Terakura, *Chem. Phys. Chem.* **6** (2005) 1775.
- [74] D.W. M. Hofmann, L. Kuleshova, and B. D'Aguanno, *J. Mol. Model* **14** (2008) 225.
- [75] A. A. Kornyshev, A. M. Kuznetsov, E. Spohr, and J. Ulstrup, *J. Phys. Chem. B* **107** (2003) 3351.
- [76] N. Agmon, *Chem. Phys. Lett.* **319** (2000) 247.

- [77] J. A. White, E. Schwegler, G. Galli, and F. Gygi, *J. Chem. Phys.* **113** (2000) 4668.
- [78] I. Bako, J. Hutter, and G. Palinkas, *J. Chem. Phys.* **117** (2002) 9838.
- [79] T. Ikeda, M. Boero, and K. Terakura, *J. Chem. Phys.* **127** (2007) 074503.
- [80] T. Remsungnen, and B.M. Rode, *Chem. Phys. Lett.* **385** (2004) 491.
- [81] Y. Kameda, K. Sugarawa, T. Usuki, and O. Uemura, *Bull. Chem. Soc. Jpn.* **71** (1998) 2769.
- [82] N. Skipper, and G. Neilson, *J. Phys., Condens. Matter* **1** (1989) 4141.
- [83] R. Caminiti, G. Licheri, G. Paschina, G. Piccaluga, and G. Pinna, *J. Chem. Phys.* **72** (1980) 4522.
- [84] M. M. Probst, T. Radnai, K. Heinzinger, P. Bobb, and B. M. Rode, *J. Phys. Chem.* **89** (1985) 753.
- [85] F. Jalilehvand, D. Spangberg, P. Lindqvist-Reis, K. Hermanson, I. Person, and M. Sandstrom, *J. Am. Chem. Soc.* **123** (2001) 431.
- [86] G. Licheri, G. Piccaluga, and G. Pinna, *J. Chem. Phys.* **64** (1976) 2437.
- [87] A. M. Chmelnick, and D. Fiat, *J. Am. Chem. Soc.* **93** (1971) 2875.
- [88] C. Sosa, J. Andzelm, B.C. Elkin, E. Wimmer, K.D. Dobbs, and D.A. Dixon, *J. Phys. Chem.* **96** (1992) 6630.
- [89] A. E. Reed, L.A. Curtiss, and F. Weinhold, *Chem. Rev.* **88** (1988) 899.
- [90] N. Metropolis, and S. Ulam, *J. Am. Stat. Ass.* **44** (1949) 335.
- [91] D. F. Parsons, and B. W. Ninham, *J. Phys. Chem. A* **113** (2009) 1141.
- [92] R. Kumar, J. R. Schmidt, and J. L. Skinner, *J. Chem. Phys.* **126** (2007) 204107.
- [93] K. Liu, M. G. Brown, C. Carter, R. J. Saykally, J. K. Gregory, and D. C. Clary, *Nature* **381** (1996) 501.

- [94] K. Liu, M. G. Brown, and R. J. Saykally, *J. Phys. Chem. A* **101** (1997) 8995.
- [95] J. T. Su, X. Xu, and W. A. Goddard III, *J. Phys. Chem. A* **108** (2004) 10518.
- [96] P. L. Silvestrelli, and M. Parrinello, *Phys. Rev. Lett.* **82** (1999) 3308.
- [97] M. Boero, K. Terakura, T. Ikeshoji, C.C. Liew, and M. Parrinello, *Phys. Rev. Lett.* **85** (2000) 3245.
- [98] G. H. Haggis, J. B. Hasted, and T. J. Buchanan, *J. Chem. Phys.* **20** (1952) 1452.
- [99] S. Liu, *J. Chem. Phys.* **126** (2007) 244103.
- [100] A. Holas, and N. H. March, *Phys. Rev. A* **44** (1991) 5521.
- [101] M. Torrent-Sucarrat, S. Liu, and F. De Proft, *J. Phys. Chem. A* **113** (2009) 3698.
- [102] D.A. McQuarrie, and J.D. Simon, *Physical Chemistry – A Molecular Approach* (University Science Books, California, 1997) p. 209.
- [103] The monomer dipole moment (scalar) of a water cluster is different from the total dipole moment (vector) of a water cluster or bulk water, as previously reported by Schmidt et al¹⁰⁴.
- [104] D.A. Schmidt, R. Scipioni, and M. Boero, *J. Phys. Chem. A* **113** (2009) 7725.
- [105] C. G. Sinn, R. Dimova, and M. Antonietti, *Macromolecules* **37** (2004) 3444.
- [106] T. Ohki, M. Harada, and T. Okada, *J. Phys. Chem. B.* **112** (2008) 11863.
- [107] H. D. Burrows, D. Costa, M. L. Ramos, M. G. Miguel, M. H. Teixeira, A. A. C. C. Pais, A. J. M. Valente, M. Bastos, and G. Bai, *Phys. Chem. Chem. Phys.* **14** (2012) 7950.
- [108] H. Li, K. Tsay, H. Wang, J. Shen, S. Wu, J. Zhang, N. Jia, S. Wessel, R. Abouatallah, N. Joos, and J. Schrooten, *J. Power Sources* **195** (2010) 8089.
- [109] P. Hänggi and M. Borkovec, *Rev. Mod. Phys.* **62** (1990) 251.

- [110] J. M. Martinez, J. H. Cobos, H. Martin, R. R. Pappalardo, I. O. Blake, E. S. Marcos, *J. Chem. Phys.* **112** (2000) 2339.
- [111] C. Sosa, J. Andzelm, B. C. Elkin, E. Wimmer, K. D. Dobbs, and D. A. Dixon, *J. Phys. Chem.* **96** (1992) 6630.
- [112] C Peng, P. Y. Ayala, and H. B. Schlegel, *J. Comp. Chem.* **17** (1996) 49.
- [113] J. M. Martinez, R. R. Pappalardo, and E. S. Marcos, *J. Am. Chem. Soc.* **121** (1999) 3175.
- [114] T. N. Truong D. G. Truhlar, K. K. Baldridge, M. S. Gordon, and R. Steckler, *J. Chem. Phys.* **90** (1989) 7137.
- [115] F. Weinhold, and C. Landis, *Valency and Bonding*, Cambridge University Press, Cambridge, 2005.
- [116] H. S. Kuncoro, M. Sakaue, H. Nakanishi, H. Kasai, and H. K. Dipojono, *JPSJ.* **80** (2011) 024601.
- [117] M. Uudsemaa, and T. Tamm, *Chem. Phys. Lett.* **400** (2004) 54.
- [118] M. Cossi, N. Rega, G. Scalmani, and V. Barone, *J. Comp. Chem.* **24** (2003) 669.
- [119] H. W. Horn, W. C. Swope, J. W. Pitera, J. D. Madura, T. J. Dick, G. L. Hura, and T. Head-Gordon, *J. Chem. Phys.* **120** (2004) 9665.
- [120] Y. Marcus, *J. Chem. Soc., Faraday Trans. 1.* **83** (1987) 339.
- [121] R. S. Mulliken, *J. Chem. Phys.* **23** (1955) 1833.
- [122] T. A. Keith, and R.F.W. Bader, *Chem. Phys. Lett.* **194** (1992) 1.
- [123] A. E. Reed, R. B. Weinstock, and F. Weinhold, *J. Chem. Phys.* **83** (1985) 735.
- [124] F. D. Proft, C.V. Alsenoy, A. Peeters, W. Langenaeker, and P. Geerlings, *J. Comput. Chem.* **23** (2002) 1198.

- [125] C. I. Bayly, P. Cieplak, W. D. Cornell, and P. A. Kollman, *J. Phys. Chem.* **97** (1993) 10269.
- [126] R. G. Parr and W. Young, *Density-Functional Theory of Atoms and Molecules*, Oxford University Press, New York, 1989.
- [127] R. N. Barnett, U. Landman, C. L. Cleveland, and J. Jortnerr, *J. Chem. Phys.* **88** (1988) 4421.
- [128] E. I. Solomon, M. J. Baldwin, and M. D. Lowery, *Chem. Rev.* **92** (1992) 521.
- [129] B. N. Figgis and M. A. Hitchman, *J. Chem. Edu.* **79** (2002) 1072.
- [130] C. Møller and M. S. Plesset, *Phys. Rev.* **46** (1934) 618.
- [131] S. Yoo, E. Apra, X. C. Zeng, and S. S. Xantheas, *J. Phys. Chem. Lett.* **1** (2010) 3122.
- [132] K. R. Glaesemann and M. W. Schmidt, *J. Phys. Chem. A* **114** (2010) 8772.
- [133] T. S. Almeida, K. Coutinho, B. J. C. Cabral, and S. Canuto, *J. Chem. Phys.*, **128**, 014506.
- [134] R. D. Amos, J. S. Andrews, N. C. Handy, and P. J. Knowles, *Chem. Phys. Lett.* **185** (1991) 256.
- [135] M. L. Leininger, W. D. Allen, H. F. Schaefer III, and C. D. Sherrill, *J. Chem. Phys.* **112** (2000) 9213.
- [136] N. M. O'Boyle, A. L. Tenderholt, and K. M. Langner., *J. Comp. Chem.* **29** (2008) 839.
- [137] P. Hunt, M. Sprik, and R. Vuilleumier, *Chem. Phys. Lett.* **376** (2003) 68.
- [138] K. Nakamoto, *Infrared and Raman Spectra of Inorganic and Coordination Compounds*, A John Wiley & Sons, Inc., New Jersey, 2009.
- [139] Gaussian ver. 03 (Gaussian Inc., Wallingford, CT, 2004).

- [140] B. A. Hess, L. J. Schaad, P. Carsky, and R. Zahradnik, *Chem. Rev.* **86** (1986) 709.
- [141] K. Ando, and J. T. Hynes, *J. Phys. Chem. B* **101** (1997) 10464.
- [142] H. B. Schlegel, *Advan. Chem. Phys.* **67** (1987) 249.
- [143] J. D. Head, *J. Comp. Chem.* **11** (2004) 67.
- [144] J. Baker, A. Schemer, and J. Andzelm, *Chem. Phys. Lett.* **216** (1993) 380.
- [145] S. Simon, M. Duran, and J. J. Dannenberg, *J. Chem. Phys.* **105** (1996) 11024.
- [146] K. Fukui, *Angew. Chem. Int. Ed. Engl.* **21** (1982) 801.
- [147] G. Klopman, *J. Am. Chem. Soc.* **90** (1968) 223.
- [148] L. Turi, *J. Chem. Phys.* **110** (1999) 10364.
- [149] C. G. Elles, C. A. Rivera, Y. Zhang, P. A. Pieniazek, and S. E. Bradforth, *J. Chem. Phys.* **130** (2009) 084501.
- [150] J. R. Ferraro, and A. Walker, *J. Chem. Phys.* **42** (1964) 1278.
- [151] R. Camaniti, G. Licheri, G. Piccagula, and G. Pinna, *J. Chem. Phys.* **69** (1978) 1.
- [152] W. Bol, and T. Welzen, *Chem. Phys. Lett.* **49** (1977) 189.
- [153] A. Munoz-Paez, R. R. Pappalardo, and E. S. Markos, *J. Am. Chem. Soc.* **117** (1995) 11710.
- [154] P. L. W. Tregenna-Piggott, H. Weihe, and A-L. Barra, *Inorg. Chem.* **42** (2003) 8504.
- [155] H. Ohtaki, and T. Radnai, *Chem. Rev.* **93** (1993) 1157.
- [156] M. Benfatto, J. A. Solera, J. G. Ruiz, and J. Chaboy, *Chem. Phys.* **282** (2002) 441.
- [157] C. F. von Weizsäcker, *Z. Phys.* **96** (1935) 431.

- [158] S. Liu, J. Chem. Phys. **126** (2007) 244103.
- [159] A. Oszko, J. Kiss, and I. Kiricsi, Phys. Chem. Chem. Phys. **1** (1999) 2565.

Appendix

Gaussian 03 Program Input

1.1 An example for optimization

Following is an example input program for fully optimization for $[\text{Cr}(\text{H}_2\text{O})_6]^{3+}$ system.

```
#p uB3LYP/GEN Opt
```

```
Cr[(h2o)6]3+
```

```
3 4
```

```
Cr1 -0.00165 -0.00052 0.00009 H17 -0.86231 2.59169 -0.77824
O2 0.24344 -1.13219 -1.78816 H18 0.87147 -2.58935 0.77844
O3 -0.24717 1.13094 1.78837 H19 0.69442 -1.77307 2.09278
O4 -2.06260 -0.65365 0.12595
O5 2.05983 0.65340 -0.12579 O H 0
O6 -0.61590 1.72516 -1.13014 6-311++G(d,p)
O7 0.62726 -1.72175 1.12924 ****
H8 1.06817 -1.24986 -2.28034 Cr
H9 -0.41487 -1.71754 -2.18840 DGDZVP
H10 -1.07031 1.24505 2.28400 ****
H11 0.41138 1.71649 2.18793
H12 -2.80448 -0.31732 -0.39530
H13 -2.41730 -1.33450 0.71398
H14 2.41378 1.33517 -0.71316
H15 2.80224 0.31530 0.39351
H16 -0.68809 1.77623 -2.09336
```

1.2 An example for partial optimization

Following is an example input program for partial optimization for $[\text{Cr}(\text{H}_2\text{O})_6]^{3+}$ system.

```
#p uB3LYP/GEN Opt(ModRedundant)
```

```
Cr[(h2o)6]3+ Orietation-Z
```

```
3 4
```

```
Cr
```

```
O1 Cr 2.00650 H -2.58342 0.00204 0.77878
```

```
x 2.00618 0.00000 0.00823 H -2.57308 -0.00029 -0.80306
```

```
H1 O1 0.9761 Cr 125.859 x 90.996
```

```
H2 O1 0.9761 H1 108.253 x 130.302 2 1 2.00650 s 50 0.1
```

```
O3 2.00618 0.00000 0.00823
```

```
O 0.00021 -0.00015 -2.00651 O H 0
```

```
O2 -0.00040 -2.00616 0.00082 6-311++G(d,p)
```

```
O 0.00058 2.00617 -0.00092 ****
```

```
O -2.00619 0.00536 -0.00835 Cr
```

```
H 0.01367 -0.79099 -2.57857 DGDZVP
```

```
H 0.01449 0.79097 -2.57814 ****
```

```
H 0.79076 -2.57781 0.01214
```

```
H -0.79086 -2.57878 -0.01078
```

```
H 0.79125 2.57847 0.01010
```

```
H -0.79059 2.57781 -0.01119
```

```
H 2.57332 0.00207 0.80280
```

```
H 2.58322 -0.00213 -0.77906
```

Curriculum Vitae (CV)

Handoko Setyo Kuncoro

List of Publications:

1. H. S. Kuncoro, R. Belkada, M. David, H. Nakanishi, H. Kasai, E. S. Dy, and H. K. Dipojono, *A Theoretical Study on the Formation, Binding Energy and Monomer Dipole Moment of Small Water Cluster Systems*, e-Journal of Surface Science and Nanotechnology, **7** (2009) 871.
2. H. S. Kuncoro, M. Sakaue, H. Nakanishi, H. Kasai, H. K. Dipojono, *First-Principles Investigation on Ionization Strength, Volume Expansion, and Water Rotational Rigidity of Small Water Cluster Systems Formed around Sodium(I), Calcium(II), and Iron(II) Ions*, Journal of Physical Society of Japan, **80** (2011) 024601.
3. S. M. Aspera, S. Adachi, H. Kasai, H. S. Kuncoro, H. K. Dipojono, *A DFT-based Analysis on H₂O Molecule Adsorption and Dissociation on the Rutile TiO₂ (110) and (100) Surfaces*, Journal of the Vacuum Society of Japan, **55** (2012) 341.
4. H. S. Kuncoro, M. Sakaue, H. Kasai, *The Effects of Charge Density Distributions of Metal Ions on Single Water Molecule Dissociation in Dehydrated M[(H₂O)₆]³⁺ Systems*, PCCP, (Under revision 2012).

List of International Conferences:

1. H. S. Kuncoro, E. S. Dy, H. Kasai, *The electronic properties of $(H_2O)_n$, $Fe^{2+}(H_2O)_n$, $Fe^{3+}(H_2O)_n$ and $Ca^{2+}(H_2O)_n$* , International Conference on Quantum Simulators and Design (QSD2008), Tokyo, Japan, 31 May – 4 June 2008.
2. H. S. Kuncoro, M. D. Yadao, R. Belkada, H. Nakanishi, H. Kasai, *A DFT-based Study of Small Water Cluster System*, Annual Meeting/Autumn Meeting (2009), The 64th JPS Annual Meeting, Tokyo, Japan, 27-30 March 2009.
3. H. S. Kuncoro, R. Belkada, M. David, E. S. Dy, H. Nakanishi, H. K. Dipojono, and H. Kasai, *A Theoretical Study on the Formation and Binding Energies of Small Water Cluster Systems*, The 11th ISSP International Symposium (ISSP-11) on Hydrogen and Water in Condensed Matter Physics, Chiba, Japan, 12-16 October 2009.
4. H. S. Kuncoro, R. Belkada, M. David, E. S. Dy, H. Nakanishi, H. K. Dipojono, and H. Kasai, *The Binding Energy: A Molecular Assembly Perspective On Small Water Cluster System*, Second International Symposium On Atomically Controlled Fabrication Technology, Osaka, Japan, November 2009.
5. H. S. Kuncoro, M. Sakaue, H. Nakanishi, H. K. Dipojono, and H. Kasai, *A DFT Investigation on Ionization Strength, Volume Expansion, and Water Rotational Rigidity of Small Water Cluster Systems Formed around Sodium(I), Calcium(II), and Iron(II) Ions*, International Conference on Core Research and Engineering Science and Advanced Material, Osaka, Japan, May 30th – June 4th, 2010.
6. H. S. Kuncoro, H. Kasai, *BOMD study on Structure of Small Water Clusters near 353.15K*, Multi-scale material modeling 1st Symposium (16th Symposium–Molecular Dynamics), 23-24 May 2011.
7. H. S. Kuncoro, M. Sakaue, and H. Kasai, *Interaction of Trivalent Transition Metal Ions (Cr, Mn, Fe, Co, Ni) with Water Molecules*, Physical Society of Japan – Fall Meeting, Toyama, Japan, September 2011.
8. H. S. Kuncoro, M. Sakaue, and H. Kasai, *Interactions of triply charged metal Cr(III), Mn(III), Fe(III), Co(III) and Ni(III) ions with water*, International Symposium on Materials Science and Innovation for Sustainable Society Eco-materials and Eco-innovation for Global Sustainability (ECO-MATES 2011), Hankyu Expo park Osaka, Japan, 28-30 November, 2011.

List of International Collaboration Workshops:

1. Hanoi University of Science – Osaka University, International Workshop on Quantum Simulation 2008 (Japan), September 12th, 2008.
2. Institut Teknologi Bandung - Osaka University, Academic Research Workshop In Pursuit of an Alternative Energy Source from Hydrogen, June 30th, 2008.
3. DLSU - Osaka University, Academic Research Workshop, February 18th, 2009.
4. Osaka University - Institut Teknologi Bandung, International Workshop on Quantum Simulation and Design, March 5th, 2009.
5. Osaka University – University British of Columbia, Workshop on Fuel Cell and Surface Science, November 6th, 2009.
6. Osaka University - Kyoto University, Workshop on Water and Hydrogen Dynamics, December 2nd, 2009.
7. Osaka University - DLSU Academic Research Workshop, Workshop on Philosophy, Science and Physics, 27-18 May 2010.
8. Hanoi University of Science – Osaka University – Center for Ceramics, Scientific Workshop, November 22nd, 2010.
9. Japan-Croatia Collaborative Workshop on Dynamics of Molecules on Surface, March 3, 2011.
10. International Workshop on Applied Surface Science/Nanostructures and Fuel Cell Engineering, April 27th, 2011 (Osaka University – Institut Teknologi Bandung - The University of British Columbia).
11. Japanese – Croatian Workshop on Material Science, 6-7 October 2011, Zagreb, Croatia.

Provisional Educations

1. Engineering Physics (S1-Bachelor) – ITS Surabaya
2. Informatics (Magister Teknik) – ITB Bandung
3. Precision Science and Technology and Applied Physics (Master Engineering) – Osaka University Osaka

Training and Courses

1. Computational Material Design 16th – IIAS (Kyoto) – Japan (2010).
2. Non-Destructive Testing (ASNT) – Centre for Metal and Machine Industrial Research and Development (Bandung) – Indonesia.
3. Industrial Radiography Testing – National Atomic Energy Agency (Jakarta) – Indonesia.
4. Risk-based Inspection – B4T/ITB (Bandung) – Indonesia.
5. Uncertainty measurement in Testing Laboratory – National Standardization Agency – BSN (Bandung) – Indonesia.
6. Internal Auditor – SNI 19-17025-2000 – National Standardization Agency – BSN (Bandung) – Indonesia.

Experiences

1. Referee of PRB Journal (2010 - 1 paper, 2012 – 1 paper).
2. Executive Staff, Research and Development Division – Fuboru Indonesia, Co. Ltd., Surabaya – Indonesia (1999 – 2000).
3. Executive Staff, (Non-Destructive Testing) Technical Inspection Division – Centre for Metal and Machine Industrial Research and Development, Bandung – Indonesia (2000 – 2002).
4. Executive Staff, Advance Ceramics, Glass and Email Research Facilities Section – Center for Ceramics, Agency for Research and Development Industry – The Indonesia Ministry of Industry, Bandung – Indonesia (2002 – present).
5. Special Researcher, Osaka University (2012-2013).

Acknowledgment

These works have been supported by the Global Centre of Excellent (G-COE) Program (H08) “Center of Excellence for Atomically Controlled Fabrication Technology” Grant-in-Aid for Scientific Research on Innovative Areas Program (2203-22104008) and Scientific Research C (22510107) program and the Ministry of Education, Culture, Sports, Science and Technology of Japan (MEXT) through Quantum Engineering Design Course Program. Some of the calculations presented here were performed using the computer facilities of the Institute of Solid State Physics (ISSP) Super Computer Center (University of Tokyo), the Yukawa Institute (Kyoto University), The Cybermedia Center (Osaka University), and the Japan Atomic Energy Research Institute (ITBL, JAERI). HSK wishes to thank the MEXT for the Monbukagakusho scholarship, and thanks to Prof. Hideaki Kasai, Ass. Prof. Wilson A. Dino, Dr. Mamoru Sakaue, Dr. Nakanishi-sensei, and all staff and students in Kasai Laboratory for their lectures, guidances and assistances, and also HSK wishes to thank the Indonesian Ministry of Industry, which allowed him to study in Japan. We must acknowledge the kindness Prof. Morikawa Y., Prof. Fukutani, Prof. A. Yagi, and Prof. T. Kubo for taking the time from your busy schedule to provide invaluable recommendation for my doctoral dissertation.

